The Journal of Physiology

# A physiological model of the inflammatory-thermal-pain-cardiovascular interactions during an endotoxin challenge

Atanaska Dobreva[1,2,†], Renee Brady-Nicholls[3,†], Kamila Larripa[4], Charles Puelz[5], Jesper Mehlsen[6] and Mette S. Olufsen[1]

[1]*Department of Mathematics, North Carolina State University, Raleigh, NC, USA*
[2]*School of Mathematical and Natural Sciences, Arizona State University, Glendale, AZ, USA*
[3]*Department of Integrated Mathematical Oncology, H. Lee Moffitt Cancer Center and Research Institute, Tampa, FL, USA*
[4]*Department of Mathematics, Humboldt State University, Arcata, CA, USA*
[5]*Department of Pediatrics, Section of Cardiology, Texas Children's Hospital and Baylor College of Medicine, Houston, TX, USA*
[6]*Section for Surgical Pathophysiology, Rigshospitalet, Copenhagen, Denmark*

Edited by: Harold Schultz & Eleonora Grandi

**Key points**

- Inflammation in response to bacterial endotoxin challenge impacts physiological functions, including cardiovascular, thermal and pain dynamics, although the mechanisms are poorly understood.
- We develop an innovative mathematical model incorporating interaction pathways between inflammation and physiological processes observed in response to an endotoxin challenge.
- We calibrate the model to individual data from 20 subjects in an experimental study of the human inflammatory and physiological responses to endotoxin, and we validate the model against human data from an independent study.
- Using the model to simulate patient responses to different treatment modalities reveals that a multimodal treatment combining several therapeutic strategies gives the best recovery outcome.

**Abstract** Uncontrolled, excessive production of pro-inflammatory mediators from immune cells and traumatized tissues can cause systemic inflammatory conditions such as sepsis, one of the ten leading causes of death in the USA, and one of the three leading causes of death in the intensive care

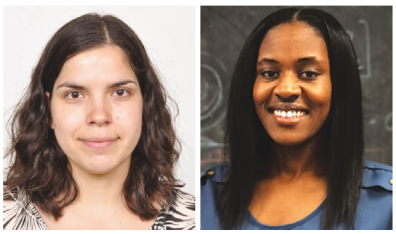

**Atanaska Dobreva** was born and grew up in Bulgaria. She earned a Bachelor of Arts degree in Mathematics and Economics from Marymount University and a PhD in Mathematics from Florida State University. During her postdoc at North Carolina State University, Atanaska studied interactions between inflammation and physiological processes using mathematical modelling and analysis. She is currently a Postdoctoral Scholar at Arizona State University where she is extending her models on the autoimmune response to study retinal degeneration research. **Renee Brady-Nicholls** was born in Ontario, Canada and grew up in South Florida. She earned her Bachelor of Science in Mathematics from Florida A&M University and her PhD in Applied Mathematics from North Carolina State University. For her PhD, she worked on developing patient-specific models for analyzing the impact of the inflammatory response to endotoxin on the cardiovascular system. She is currently a Research Instructor at Moffitt Cancer Center where she continues to develop patient-specific models, identifying patient-specific longitudinal biomarkers in cancer.

[†]These authors contributed equally to this work.

This article was first published as a preprint. Dobreva A, Brady R, Larripa K, Puelz C, Mehlsen J, Olufsen MS. 2019. A physiological model of the inflammatory-thermal-pain-cardiovascular interactions during a pathogen challenge. arXiv. https://arxiv.org/abs/1908.07611.

 DOI: 10.1113/JP280883

unit. Understanding how inflammation affects physiological processes, including cardiovascular, thermal and pain dynamics, can improve a patient's chance of recovery after an inflammatory event caused by surgery or a severe infection. Although the effects of the autonomic response on the inflammatory system are well-known, knowledge about the reverse interaction is lacking. The present study develops a mathematical model analyzing the inflammatory system's interactions with thermal, pain and cardiovascular dynamics in response to a bacterial endotoxin challenge. We calibrate the model with individual data from an experimental study of the inflammatory and physiological responses to a one-time administration of endotoxin in 20 healthy young men and validate it against data from an independent endotoxin study. We use simulation to explore how various treatments help patients exposed to a sustained pathological input. The treatments explored include bacterial endotoxin adsorption, antipyretics and vasopressors, as well as combinations of these. Our findings suggest that the most favourable recovery outcome is achieved by a multimodal strategy, combining all three interventions to simultaneously remove endotoxin from the body and alleviate symptoms caused by the immune system as it fights the infection.

(Received 8 October 2020; accepted after revision 11 January 2021; first published online 15 January 2021)
**Corresponding author** M. S. Olufsen: Department of Mathematics, North Carolina State University, Raleigh, SAS Hall 3154, Box 8205, NC 27695, USA. Email: msolufse@ncsu.edu

## Introduction

Systemic inflammation is comorbid with several diseases, including diabetes (Wei *et al*. 2016), cancer (Coussens & Werb 2002), heart disease (Yudkin *et al*. 2000) and sepsis (Tracey, 2002; Huston *et al*. 2008; Huston & Tracey, 2011; Tracey, 2011) and it plays a prominent role in eight out of the ten leading causes of death in the USA (Hoyert & Xu, 2012). The action of inflammation is multifaceted and impacts multiple organ systems, such as the digestive, respiratory, endocrine and nervous systems.

Numerous *in vivo* studies in mice and rats have examined the effects of autonomic control on the inflammatory system (Tracey, 2002, 2011). Borovikova *et al*. (2000) discovered the cholinergic anti-inflammatory pathway modulating the immune response via the local release of ACh from vagal fibres in target tissues. They found that an increase in vagal activity results in a decrease in the pro-inflammatory cytokines tumour necrosis factor (TNF-$\alpha$), interleukin 6 (IL-6) and interleukin 1$\beta$ (IL-1$\beta$). Tracey (2002; 2011) describes the effects of autonomic control on inflammation, noting that cytokine production activates afferent firing to the brain and subsequent vagal efferent activation inhibits cytokine synthesis. This inflammation-sensing and inflammation-suppressing network (dubbed the inflammatory reflex) monitors and adjusts inflammatory function via neural pathways maintaining homeostasis of the immune response. Although the above studies elucidated how autonomic control modulates inflammation, they did not discuss how inflammation impacts autonomic function controlling physiological processes.

Several studies have used systems-level mathematical modelling to explore the inflammatory response to an endotoxin challenge in rodents using models against *in vivo* experimental data. Seminal studies include contributions by Chow *et al*. (2005) investigating the acute inflammatory response to a bolus administration of the bacterial endotoxin lipopolysaccharide (LPS). This study demonstrated that three different inflammation triggers (i.e. endotoxaemia, surgical trauma and haemorrhage) engage in a universal cascade of immune signals, noting that the behaviour and magnitude of activity differ among the triggers. For example, they found that: (i) the peak concentrations of pro-inflammatory cytokines (TNF-$\alpha$ and IL-6) in surgical trauma and hemorrhage are significantly lower than in endotoxaemia and (ii) surgery-induced inflammation leads to a higher peak concentration of the anti-inflammatory mediator IL-10 compared to endotoxaemia. Later, Prince *et al*. (2006) showed that the classic LPS response pathway via the immune receptor CD14 is not involved in inflammation and organ damage after surgical trauma or haemorrhagic shock, and Daun *et al*. (2008) found that tissue damage levels in rats can be associated with the cytokine levels.

Agent-based models (ABMs) also describe the acute inflammatory response (Dong *et al*. 2010; Brown *et al*. 2011). This model type describes the behaviour of autonomous agents (components of the complex system) and predicts the system's aggregate behaviour (An, 2006). Dong *et al*. (2010) used an ABM in which the agents are immune cells (macrophages and helper T cells) and interleukin cytokines to predict inflammation propagation.

Although the above investigations revealed essential features of the immune reaction to pathogens in rodents (Chow *et al.* 2005; Prince *et al.* 2006; Daun *et al.* 2008) and humans (Dong *et al.* 2010), they did not elucidate how the inflammatory system interacts with the cardiovascular, thermal and pain systems. Moreover, the inflammatory pathways differ between rodents and humans (Seok *et al.* 2013) and rodents tolerate much higher pathogen levels (Fink, 2014). Copeland *et al.* (2005) demonstrated this by administering LPS to humans and mice, at doses 2 ng $kg^{-1}$ of body weight for humans and 500 ng $kg^{-1}$ for mice, eliciting equivalent IL-6 plasma concentrations 2 hr post-injection. Their results showed that humans experienced fever, increased heart rate (HR) and systolic blood pressure (SBP), whereas the mice had no fever or changes in HR and SBP. These experimental observations demonstrate that investigations in mice do not have direct applicability to humans.

Several studies have used models to examine inflammatory-cardiovascular communication in humans (Foteinou *et al.* 2011; Scheff *et al.* 2011; McDaniel *et al.* 2019; Yamanaka *et al.* 2019). Foteinou *et al.* (2011) employed a multiscale model to predict the parasympathetic activity and HR in human subjects who received a bolus dose of LPS (2 ng $kg^{-1}$ of body weight) alone or combined with an epinephrine infusion. Scheff *et al.* (2011) expanded this model by incorporating transcriptional immune activity via hormonal circadian rhythms in cortisol and melatonin and showed that circadian variability in inflammation correlates with daily HR patterns. Although these investigations reflect the complexity of immune dynamics at the transcriptional level, they do not explain how the systemic spread of inflammation, via cytokines and immune cells in the circulation, affects cardiovascular function. Moreover, these studies do not assess how inflammation impacts thermal and pain regulation and the subsequent effects on haemodynamics. McDaniel *et al.* (2019) and Yamanaka *et al.* (2019) explored the effects of systemic inflammation on blood pressure (BP) and HR. However, The first study did not calibrate the immune subsystem with experimental data, and in the second study- calibration was done with data from mice, not humans. Also, Yamanaka *et al.* (2019) did not incorporate temperature or pain responses.

The present study develops the first mathematical model successfully capturing the response to a one-time LPS challenge in healthy individuals. The model is calibrated to data from 20 healthy young individuals using data reported by Janum *et al.* (2016) and validated against data reported by Copeland *et al.* (2005). We use this model to simulate the response to a sustained LPS and various treatments, including LPS adsorption, antipyretics and vasopressors, as well as a combination of these interventions. Our results suggest that untreated, sustained endotoxaemia leads to abnormally elevated HR and low BP. The simulation analysis of treatments indicates that to remedy the detrimental effects of an infection, the most effective approach is to administer a multimodal treatment simultaneously removing LPS from the body and alleviating symptoms caused by the immune reaction to the infection.

## Methods

### Ethical approval

The present study analyzes previously published data reported by Janum *et al.* (2016) and Copeland *et al.* (2005). Individual anonymized data from Janum *et al.* (2016) were made available for this analysis by one of the coauthors (J. Mehlsen). The data-handling committee at Bispebjerg and Frederiksberg Hospitals approved the sharing of anonymized data. Average population data from the Copeland study were digitized from the manuscript. The Regional Committee on Health Research Ethics and the Regional Data Monitoring Board approved the experimental protocol used in the Janum study, and the Institutional Review Board at the UMDNJ-Robert Wood Johnson Medical School approved the experimental protocol used in the Copeland study. For both studies, all subjects provided their written consent to participate.

### Experimental data

For the present study, we use cytokine and physiological data from the two studies mentioned above. The model is calibrated using subject-specific data from Janum for 20 healthy young men and is subsequently validated using averaged data reported in the Copeland study.

**Study population.** The Janum study includes 20 healthy male adults aged 18–35 years who received a low bolus dose of LPS (2 ng $kg^{-1}$). Exclusion criteria include smoking, obesity, daily intake of medication and splenectomy. From the Copeland study, we extracted data administering the same low bolus dose of LPS (2 ng $kg^{-1}$) to 10 human subjects aged 18–40 years. Exclusion criteria for participation include chronic disease history (e.g., cancer, rheumatoid arthritis, heart disease, hypertension) or a history of abnormalities affecting the immune system (e.g., the liver and kidneys, endocrine system or neural system).

**Experimental protocol.** Both studies followed a similar experimental protocol. A 2 ng $kg^{-1}$ dose of LPS derived from *Escherichia coli* was administered I.V., and the systemic inflammatory response, body temperature, HR and BP were measured. Figure 1 shows the detailed experimental protocol for each study.

The Janum study contains data recorded 2 hr before the endotoxin injection and then hourly for 6 hr, whereas the Copeland study includes data recorded hourly for 9 hr post endotoxin injection. In addition to measuring cytokines and cardiovascular markers, the Janum study applied a heat stimulus to the non-dominant thigh at varying temperatures (45, 46, 47 and 48 °C) for 5 s, followed by a period at 32 °C to evaluate pain perception. Subjects were asked to rate each heat stimulus on a scale from 0 (*no pain*) to 10 (*worst imaginable pain*). Pain perception was measured using an algometer (Somedic AB, Hörby, Sweden) in which pressure was applied manually at increasing kPa. When participants indicated that they reached their pain threshold, the algometer value was recorded.

Both studies collected blood samples to measure plasma levels of pro-inflammatory cytokines (TNF-$\alpha$, IL-6 and IL-8) and, in the Janum study, they also measured an anti-inflammatory cytokine (IL-10). They recorded SBP and temperature hourly, immediately before the blood withdrawal. SBP was measured using a sphygmomanometer on the upper arm, and the temperature was measured orally in the Janum study and rectally in the Copeland study. The Janum study extracted beat-to-beat HR values from a precordial ECG-lead, continuously over the 8 hr interval, whereas the Copeland study measured HR at discrete time points in conjunction with BP measurements. To ensure a consistent HR data format between the two studies, we sampled the continuous measurements at the same time points from 0–6 hr. Individual data for the 20 participating subjects are available from the Janum study, whereas the Copeland study reports average data (mean ± SEM) over the population. For the present study, the latter was adjusted by multiplying the SEM by the square root of the population size.

## Mathematical model

The mathematical model includes three submodels describing (i) the inflammatory response to endotoxin; (ii) the effect of inflammation on temperature, pain perception, and nitric oxide (NO); and (iii) their impact on the cardiovascular system (schematic shown in Fig. 2). The model encodes the following interactions reported by physiological studies:

- LPS-induced inflammation induces fever (Hamzic *et al.* 2013; Evans *et al.* 2015) and lowers the pain perception threshold (Janum *et al.* 2016).
- Temperature and BP modulate HR (Karjalainen & Viitasalo, 1986; Yamazaki *et al.* 1997). An increase in temperature, inducing fever, leads to an increase in HR (Cao & Morrison, 2003; Nakamura *et al.* 2004; Vayssettes-Courchay *et al.* 2005), and an increase in BP leads to a decrease in HR (Yamazaki *et al.* 1997, Nguyen *et al.* 2006).
- Changes in pain perception are associated with an increase in vascular resistance (Maixner *et al.* 1990; Bruehl *et al.* 2002; Saccò *et al.* 2013).

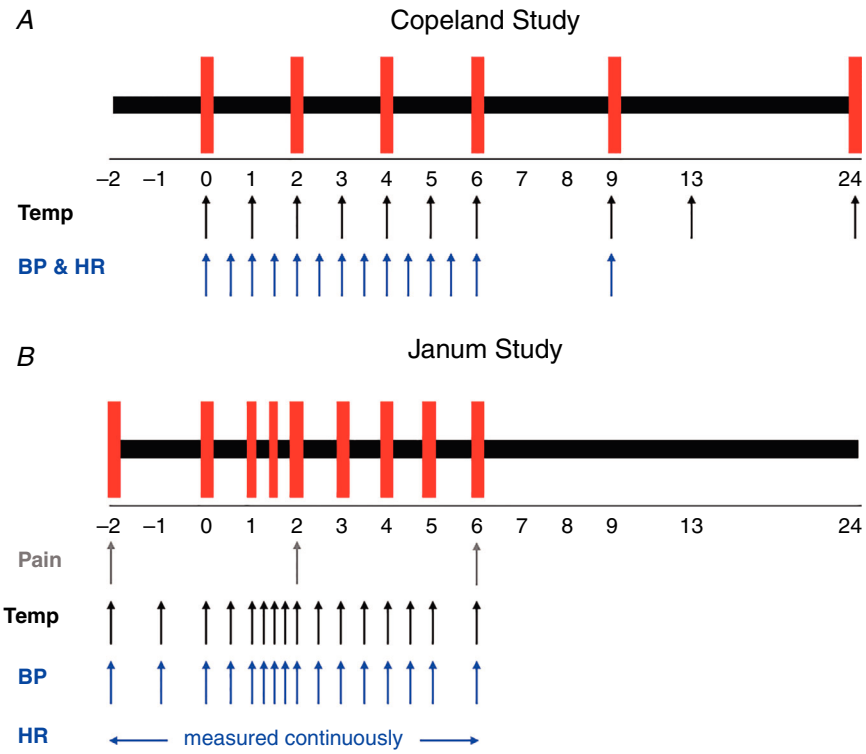


**Figure 1. Experimental protocol**
Immune mediators (TNF-$\alpha$, IL-6 and IL-8), temperature (Temp), heart rate (HR) and blood pressure (BP) were periodically collected during the studies by (*A*) Copeland *et al.* (2005) and (*B*) Janum *et al.* (2016). Note that pain perception threshold and IL-10 were only recorded in the study by Janum *et al.* (2016), and HR was continuously recorded. Recording times are represented with red vertical bars for immune mediators, black arrows for Temp, blue arrows for HR and BP, and grey arrows for pain. Zero on the time axis represents the time when LPS was administered.

- Inflammation stimulates NO synthesis causing vasodilatation (Sayk *et al.* 2008; McNeill *et al.* 2015; Salim *et al.* 2016). This response opposes the impact of pain perception on vascular resistance, but the timing of these effects is separated, and we show that both are essential to predict observed changes in BP.

**The inflammatory response to an endotoxin challenge.** Monocytes and macrophages use cytokine signalling to communicate in response to a pathogen and are an essential part of innate immunity. Bone marrow stem cells differentiate into monocytes and move into the bloodstream. The monocytes enter the connective tissue matrix, where they differentiate into macrophages, which interact with the cytokines (Pilling *et al.* 2017). Monocytes and macrophages usually are at rest, although, with stimulus from bacteria (e.g. LPS) or a virus, they become activated, and the number of macrophages increases by several orders of magnitude.

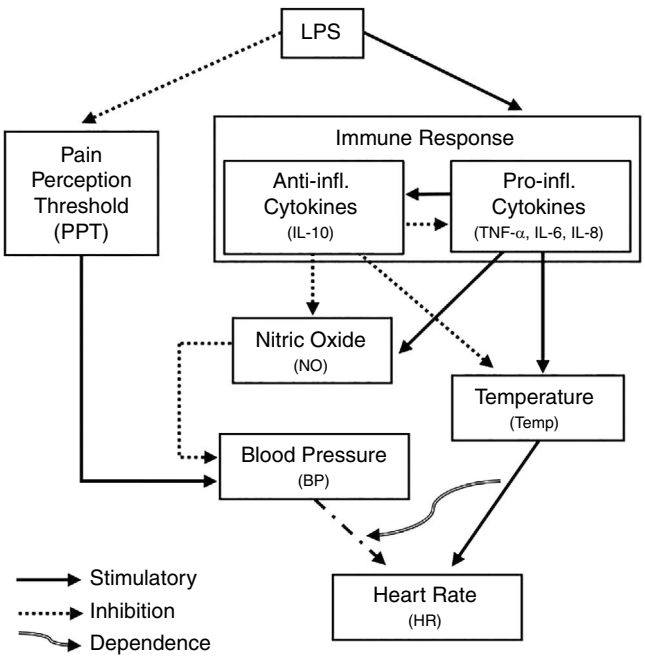


**Figure 2. Feedback diagram for human response to endotoxin challenge**
LPS administration initiates an immune cascade, as well as a decrease in the pain perception threshold. The decrease in the PT results in an increase in BP. Pro-inflammatory cytokines act as pyrogens, increasing body temperature, whereas anti-inflammatory cytokines act as antipyrogens to decrease temperature. Pro- and anti-inflammatory cytokines have opposing effects on NO production, which decreases BP via vasodilatation (decreases vascular resistance). Temperature increases HR via decrease in basal vagal tone. Elevated BP decreases HR. When BP falls to a hypotensive range, it will act to increase HR. Temperature interacts with these changes in HR via BP.

Cytokines are potent signalling molecules that regulate many processes essential to immunity and inflammation. In our previous model (Brady, 2017; Brady *et al.* 2018), we constructed a classic kinetic model of the systemic inflammatory response to an endotoxin challenge, incorporating signalling pathways illustrated in Fig. 3 (a full list of the equations is provided in the Appendix).

**The thermal, pain and NO response.**

*Thermal effects.* The binding of LPS to receptors on macrophages and other immune cells stimulates the production of pyrogenic (fever-inducing) cytokines IL-6, TNF-$\alpha$ and IL-1$\beta$, which act to induce and maintain fever. These pyrogens stimulate afferent vagal nerves terminating in the nucleus ambiguous in the brain stem, and this relays information to the hypothalamus about the ongoing inflammation and triggers the release of prostaglandins. Prostaglandins act on neurons in the preoptic nucleus of the hypothalamus, which is responsible for temperature regulation (Conti *et al.* 2004; Lazarus *et al.* 2007). TNF-$\alpha$ is a potent pyrogenic cytokine and it is one of the main cytokines implicated in septic shock. IL-6 has been shown as necessary to sustain fever (Hamzic *et al.* 2013; Evans *et al.* 2015). Conversely, IL-10 has antipyretic effects, lowering body temperature (Hamzic *et al.* 2013; Pajkrt *et al.*, 1997). The temperature regulation feedback is modelled as a function of TNF-$\alpha$, IL-6 and IL-10 by

$$\frac{d\mathrm{Temp}}{dt} = \frac{1}{\tau_1}\Big[-\mathrm{Temp} + T_b + k_T(T_M - T_b)\big(k_{T\mathrm{TNF}} H_T^U(\mathrm{TNF} - w_{\mathrm{TNF}}) + k_{T6} H_T^U(\mathrm{IL6} - w_{\mathrm{IL6}}) - k_{T10}\big(1 - H_T^D(\mathrm{IL10} - w_{\mathrm{IL10}})\big)\big)\Big], \quad (1)$$

where Temp is temperature, $T_b$ and $T_M$ is the respective baseline and maximum temperatures, and $\tau_1$, $k_T$, $k_{T\mathrm{TNF}}$, $k_{T6}$, $k_{T10}$ are rate constants. The baseline values of the cytokines are given by $w_X$, for $X \in \{\mathrm{TNF, IL6, IL10}\}$, and the up- and down-regulation of $Y$ by $X$ are described by the equations $H_Y^U(X) = \frac{X^h}{\eta_{YX}^h + X^h}$ and $H_Y^D(X) = \frac{\eta_{YX}^h}{\eta_{YX}^h + X^h}$, respectively. The half-saturation value is given by $\eta_{YX}$ and the exponent $h$ regulates the Hill function steepness.

*Pain threshold (PT).* Sensory neurons at the site of infection are stimulated in the presence of inflammation and alter signalling to the central nervous system (CNS) through vagal afferent fibres (Lai *et al.* 2017). Nociceptors are essential mediators of pain perception (Pinho-Ribeiro *et al.* 2017) and have nerve endings terminating near macrophages and other immune cells. Nociceptors sense immune signals such as TNF-$\alpha$ and IL-6 (Chavan *et al.* 2017), although they can also be activated by pathogens directly. Previous studies (Benson *et al.* 2012; Wegner *et al.* 2014; Janum *et al.* 2016) have shown a dose-dependent

relationship between pain perception and inflammation. Thus, we model the PT as

$$\frac{d\mathrm{PT}}{dt} = -\,k_{\mathrm{PT}E}\,E\,\mathrm{PT} + k_{\mathrm{PT}}\,(\mathrm{PT_b} - \mathrm{PT})\,, \qquad (2)$$

where $k_{PTE}$ and $k_{PT}$ are rate constants, $\mathrm{PT_b}$ is the baseline PT, and $E$ is the endotoxin. In response to the endotoxin, the PT decreases, slowing down as the endotoxin level falls.

*Nitric Oxide (NO).* The endothelium cells lining the blood vessels use NO signalling to interact with nearby smooth muscle cells, relaxing with increased release of NO (Lundberg *et al.* 2015). NO has direct and indirect microbial effects, including inhibition of pathogen proliferation (Bogdan, 2001; Tripathi *et al.* 2007; Bogdan, 2015). As part of the inflammation pathway, upon signalling from toll-like receptors or inflammatory cytokines, macrophages produce inducible NO synthase, which affects their phenotype and leads to NO production (McNeill *et al.* 2015). Monocytes initiate the NO synthesis 2–4 hr after receiving the stimulus (Park & Pyo, 2013). NO production is upregulated by TNF-$\alpha$ (Salim *et al.* 2016) and downregulated by IL-10 (Chesrown *et al.* 1994; Haskó *et al.* 1996). We model cytokine-mediated NO dynamics as

$$\frac{dN}{dt} = k_{NM}\,M_A\left(\frac{\mathrm{TNF}(t-\kappa)^{h_{\mathrm{NTNF}}}}{\mathrm{TNF}(t-\kappa)^{h_{\mathrm{NTNF}}} + \eta_{\mathrm{NTNF}}^{h_{\mathrm{NTNF}}}}\right) \times \left(\frac{\eta_{N10}^{h_{N10}}}{\mathrm{IL10}(t-\kappa)^{h_{N10}} + \eta_{N10}^{h_{N10}}}\right) - k_N N. \qquad (3)$$

Here, $\kappa$ represents the delay in activation/inhibition of NO from TNF-$\alpha$ and IL-10, $k_{NM}$ and $k_N$ are rate constants, and $\eta_{\mathrm{NTNF}}$, $\eta_{N10}$, $h_{\mathrm{NTNF}}$ and $h_{N10}$ are Hill function parameters determining the half-saturation value and steepness of the response.

**Effects on cardiovascular dynamics.** The cardiovascular system is continually regulated to maintain homeostasis (ensuring adequate oxygen perfusion at stable resting BP). The body maintains this state via the autonomic control system modulating vascular compliance, resistance, cardiac contractility and HR. The baroreflex branch of the autonomic control system consists of parasympathetic and sympathetic signalling, primarily responding to changes in SBP in the aortic arch and carotid sinuses (Arndt *et al.* 1977).

The vagal nerve is the primary pathway for parasympathetic signalling. An increase in parasympathetic signalling leads to a decrease in HR (Warner & Cox, 1962) via ACh release, primarily in the sinoatrial node. Preganglionic sympathetic nerve fibres travel through the spinal cord, synapsing with postganglionic fibres. A decrease in SBP stimulates noradrenaline release, which causes smooth muscle contraction, increasing the peripheral vascular resistance and decreasing the vascular wall compliance. In addition, sympathetic stimulation further increases HR as well as cardiac contractility.

The baroreflex response to changes in SBP acts within seconds, but basal activity in both efferent pathways (parasympathetic ∼20% and sympathetic ∼80% (Korner *et al.* 1976; Randall *et al.* 2019)) are present even in the absence of a stimulus (change in SBP). Because the data

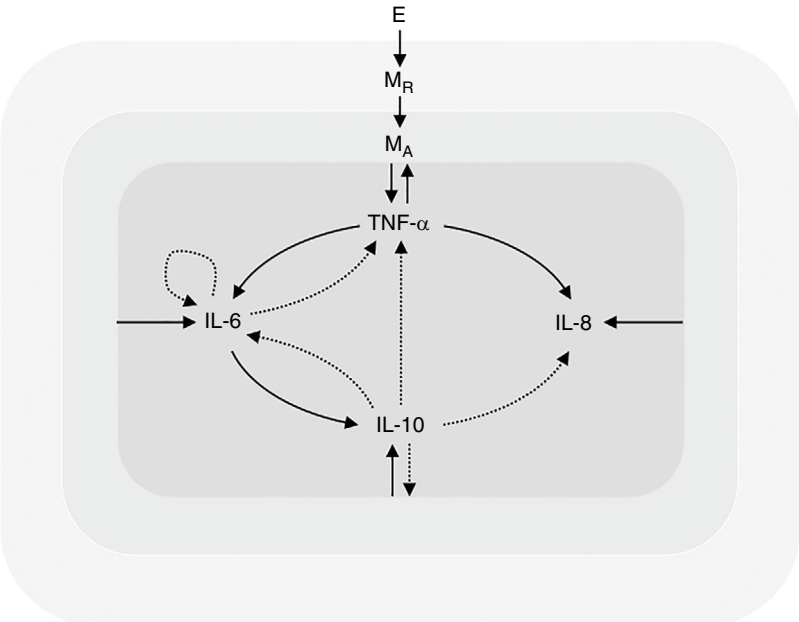


**Figure 3. Immune interactions in response to endotoxin challenge**
Endotoxin (E) administration results in the activation of monocytes (MR→MA). Activated monocytes (MA) secrete mediators that induce further immune activation (TNF-$\alpha$, IL-6 and IL-8). These pro-inflammatory mediators stimulate the production of IL-10, which regulates the immune response as an anti-inflammatory mediator. IL-6 also exhibits anti-inflammatory effects because it downregulates the synthesis of TNF-$\alpha$ and its own release.

are measured over hours, it is impossible to track the fast regulation by the autonomic system. Nevertheless, we can track slow changes in baseline signalling, which is known to change throughout the day (Shinar *et al.* 2006), but probably also in response to other factors.

In addition to the neural response, haemodynamics is also controlled locally via autoregulation. One component to this control is the response to changes in NO (a potent vasodilator) and the release of catecholamines from the adrenal medulla. To describe this, we develop a cardiovascular model producing SBP and HR as functions of changes in pain, temperature and NO levels.

*Cardiovascular model.* The model only accounts for significant BP and HR changes over hours (i.e., it does not incorporate beat-to-beat beating of the heart and respiratory dynamics). The cardiovascular model is limited to the systemic circulation and, similarly to our previous study (Williams *et al.* 2019), we model the cardiovascular system as an electrical circuit with capacitors and resistors. Our model (Fig. 4) includes two arterial compartments (large and small arteries) and two venous compartments (large and small veins). Each compartment is associated with a pressure($p$, mmHg), volume ($V$, mL) and elastance ($El$, mmHg mL$^{-1}$), and compartments are separated by resistors ($R$, mmHg s mL$^{-1}$).

The cardiovascular model relates flow ($q$, mL s$^{-1}$), volume ($V$, mL) and pressure ($p$, mmHg) using four differential equations describing the conservation of volume via

$$\frac{dV_i}{dt} = q_{\text{in}} - q_{\text{out}}, \tag{4}$$

where $q_{\text{in}}$ is flow entering a compartment, $q_{\text{out}}$ is flow leaving the compartment and $i \in \{la, lv, sa, sv\}$ ($l$ stands for large, $s$ for small, $a$ for arteries and $v$ for veins). Between two compartments, flow is related to pressure via Ohm's law given by

$$q_i = \frac{p_{\text{out}} - p_{\text{in}}}{R_i}, \tag{5}$$

where $p_{\text{in}}$ and $p_{\text{out}}$ denote the pressure in the two surrounding compartments and $R_i$ (mmHg s mL$^{-1}$) is the resistance to flow.

For each compartment, pressure is related to volume via a pressure/volume relation

$$p - p_{\text{tis}} = El\,(V - V_{\text{un}}), \tag{6}$$

where $p_{\text{tis}}$ (mmHg) is the tissue pressure, $El$ is the elastance and $V_{\text{un}}$ is the unstressed volume. We drive the cardiovascular model by a 'non-pulsatile heart' tracking stroke volume $V_{\text{str}}$ via

$$Q \approx HV_{\text{str}}, \tag{7}$$

where $H$ (beats min$^{-1}$) is the HR and $Q$ (mL s$^{-1}$) is the cardiac output. $V_{\text{str}}$, the volume of blood the heart pumps out during one beat, is computed by

$$V_{\text{str}} = V_{\text{ED}} - V_{\text{ES}} = -\left(\frac{p_{\text{la}}}{El_M} - \frac{p_{\text{lv}}}{El_m}\right), \tag{8}$$

where $V_{\text{ED}}$ is the end-diastolic volume in the heart, $V_{\text{ES}}$ is the end-systolic volume, $p_{\text{la}}$ is pressure in the large arteries, $p_{\text{lv}}$ is pressure is pressure in the large veins, and $El_M$ and $El_m$ are the maximum and minimum elastance, respectively. All of the cardiovascular model equations are listed in the Appendix.

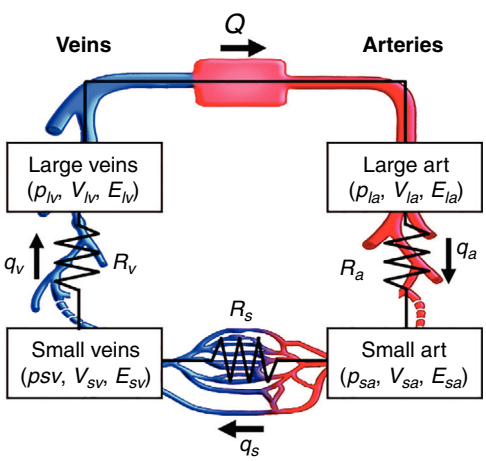


**Figure 4. Cardiovascular model**
The cardiovascular system is comprised of the small and large arteries and veins (subscripts *sa*, *la*, *sv*, *lv*). Each compartment has an associated blood pressure *p* (mmHg), volume *V* (mL), and elastance *E* (mmHg mL$^{-1}$). Flow between compartments are represented by *q* (mL s$^{-1}$), with a corresponding resistance *R* (mmHg s mL$^{-1}$) with subscripts (*a*, *v*, *s*) representing arteries, veins and peripheral vasculature.

*Cardiovascular control of HR.* As noted earlier, the relevant timescale in this study is hours, and we only consider mechanisms that regulate vascular resistance over this timescale. It has been suggested that acute pain perception stimulates sympathetic neurons, increasing peripheral vascular resistance (Saccò *et al.* 2013; Williams *et al.* 2019) and that pain intensity correlates with the increase in resistance (Maixner *et al.* 1990; Saccò *et al.* 2013). Janum *et al.* (2016) showed that subjects receiving LPS experienced enhanced pain perception as a result of a decline in the PT. Also, results by Bruehl *et al.* (2002) indicate that an increase in the PT, reducing pain perception, is associated with arterial hypertension and neurochemical pathways involving endogenous opioid substances. Finally, NO production, via a delayed response stimulated by inflammation, is a potent

inducer of vasodilatation, decreasing peripheral vascular resistance (Russell, 2006; Sayk *et al.* 2008). To generate a simple model, we include these mechanisms directly into the equation determining peripheral vascular resistance, formulated as

$$\frac{dR_s}{dt} = k_{RPT} \frac{\Gamma^2}{\Gamma^2 + \eta^2_{RPT}} - k_{RN} N - k_R (R_s - R_b), \quad (9)$$

where $\Gamma = \frac{dPT}{dt}$ is the rate of change of the pain perception threshold, $k_{RN}$ is the rate of vasodilatation by NO and $R_b$ is the baseline peripheral vascular resistance (before LPS injection) in the absence of pain and NO ($\Gamma = 0$ and $N = 0$). The rate constants are given by $k_{RPT}$, $k_{RN}$ and $k_R$. The half-saturation value of the Hill function is given by $\eta_{RPT}$. Upon administration of endotoxin, the PT decreases, resulting in an increase in $\Gamma^2$ and consequently $R_s$. As LPS decays and PT returns to its baseline value, $\Gamma^2$ approaches zero. NO begins to rise 2–4 hr after the initial inflammatory response, causing $R_s$ to decrease. Elevated vascular resistance brought about by changes in pain perception causes BP to rise. Conversely, an increase in NO lowers resistance via vasodilatation, leading to a drop in BP (Russell, 2006).

Blood pressure and body temperature influence HR (Karjalainen & Viitasalo, 1986; Yamazaki *et al.* 1997; Crandall *et al.* 2000). Blood pressure impacts HR in both the short-term (over minutes) and long-term (hours). Short-term HR regulation is primarily facilitated by the baroreflex, which increases HR by inhibiting (parasympathetic) and stimulating (sympathetic) neurons in response to a drop in BP (La Rovere *et al.* 2008). At rest, sympathetic neurons fire at ∼20% of their max rate, whereas parasympathetic neurons fire at ∼80% of their maximum rate (Korner *et al.* 1976; Randall *et al.* 2019).

*Temperature.* Studies by Cao & Morrison (2003), Nakamura *et al.* (2004) and Vayssettes-Courchay *et al.* (2005) found that the administration of endotoxin, causing a rise in body temperature, increases HR in response to stimulated basal sympathetic activity. The latter can be explained by the presence of sympathetic premotor neurons with temperature regulation functions in the rostral raphe region of the medulla oblongata, which is in close proximity to cardiac sympathetic preganglionic neurons. For healthy individuals, these neurons are not firing, whereas, during inflammation, the presence of pyrogenic cytokines in the rostral raphe region may stimulate sympathetic (Cao & Morrison, 2003; Nakamura *et al.* 2004) and inhibit parasympathetic (Crandall & Wilson, 2015) nerve activity, both increasing HR. Similar results have been found in rabbit experiments by Riedel *et al.* (1986). They showed that fever, induced by LPS, leads to a notable increase in HR. Moreover, fever increases metabolic demands via sympathetic activation, and sympathetic activity stimulates contractility, increasing stroke volume and HR. The combined effect increases cardiac output to meet the higher metabolic demand (Zhang *et al.* 2000).

*Blood pressure.* We integrate the temperature effects discussed above with BP changes because several studies (Karjalainen & Viitasalo, 1986; Yamazaki *et al.* 1997; Crandall *et al.* 2000) have found that HR is modulated by temperature and BP. Specifically, a decrease in BP (below the baseline BP) causes an increase in HR. Patients with active inflammation typically experience hypotension [i.e., SBP falls to 90–117 mmHg (Oyetunji *et al.* 2011), below the baseline]. In response, the ventricular filling is reduced, and the vessels dilate, leading to pooling of blood in the veins. These patients also experience an increase in HR essential to increase cardiac output and BP (Nguyen *et al.* 2006).

The above mechanisms are included in the equation predicting HR

$$\frac{dH}{dt} = \frac{-H + k_H (H_M - H_b) H_H^U \left(\text{Temp} - T_b\right) f(BP, BP_b) + H_b}{\tau_2}, \quad (10)$$

where

$$f(BP, BP_b) = \begin{cases} H_H^U (BP_b - BP), & \text{if } BP \leq 100 \text{ mmHg} \\ H_H^D (BP - BP_b), & \text{if } BP > 100 \text{ mmHg} \end{cases}$$

and $\tau_2$ and $k_H$ are rate constants. The effects of body temperature are included in the term $H_H^U(\text{Temp} - T_b)$, whereas modulation in response to BP is encoded in $f(BP, BP_b)$.$BP_b$ and $T_b$ represent the baseline levels of BP and temperature, respectively.

## Parameterization

Following the rigorous pipeline developed by Brady & Enderling (2019), the model is calibrated to the subject-specific data from the Janum study and validated against the averaged data from the Copeland study.

**Nominal parameters.** As noted in the Appendix, the model, comprised of submodels that predict the inflammatory, thermal, pain and cardiovascular response, is formulated using 16 delay differential equations with 88 parameters (all the parameters and their units are described in Table 1 and nominal values for all parameters are listed in Table 2). We compute nominal parameter values using a combination of literature and subject-specific values extracted from the individual data reported by Janum *et al.* (2016) and the mean data reported by Copeland *et al.* (2005).

*Inflammatory submodel.* Parameter values extracted from data include the baseline levels of cytokines

**Table 1. Descriptions and units of model parameters (par). Units reported include the number of cells (noc), temperature (Temp), heart rate (HR); blood pressure (BP), nitric oxide (NO), organ bed resistance ($R_s$), and pain threshold (PT)**

| Par. | Description | Unit | | Par. | Description | Unit | |
|---|---|---|---|---|---|---|---|
| | | | **Inflammatory submodel** | | | | |
| $k_E$ | Endotoxin decay rate | $hr^{-1}$ | # | $k_{MR}$ | $M_R$ proliferation rate | $hr^{-1}$ | * |
| $k_M$ | Rate that endotoxin activates monocytes | $hr^{-1}$ | * | $k_{MA}$ | Decay rate of $M_A$, TNF-$\alpha$ , IL6, IL8, and IL10 | $hr^{-1}$ | * |
| $k_{M\mathrm{TNF}}$ | Rate that TNF-$\alpha$ activates monocytes | $hr^{-1}$ | * | $k_{\mathrm{TNF}}$ | | | # |
| $k_{\mathrm{TNF}M}$ | $M_A$ production rate of TNF-$\alpha$, IL6, IL8 and IL10 | $\frac{pg}{ml\ hr\ noc}$ | # | $k_6$ | | | # |
| $k_{6M}$ | | | # | $k_8$ | | | # |
| $k_{8M}$ | | | # | $k_{10}$ | | | # |
| $k_{10M}$ | | | # | $w_{\mathrm{TNF}}$ | Baseline TNF-$\alpha$, IL6, IL8, and IL10 | $pg\ ml^{-1}$ | ‡ |
| $k_{6\mathrm{TNF}}$ | IL6 and IL8 synthesis in response to TNF-$\alpha$ | $\frac{pg}{ml\ hr\ noc}$ | * | $w_{\mathrm{IL6}}$ | | | ‡ |
| $k_{8\mathrm{TNF}}$ | | | * | $w_{\mathrm{IL8}}$ | | | ‡ |
| $k_{106}$ | IL10 synthesis in response to IL6 | $\frac{pg}{ml\ hr\ noc}$ | * | $w_{\mathrm{IL10}}$ | | | ‡ |
| $\eta_{ME}$ | $M_A$ half-max irt endotoxin | $ng\ kg^{-1}$ | * | $h_{ME}$ | Exp. modulating $M_A$ effect on endotoxin | - | * |
| $\eta_{M\mathrm{TNF}}$ | Half-max of $M_A$, IL6 and IL8, resp. regulating TNF-$\alpha$ | $pg\ ml^{-1}$ | * | $h_{M\mathrm{TNF}}$ | Exp. modulating $M_A$, IL6 and IL8, resp. effect on TNF-$\alpha$ | - | * |
| $\eta_{6\mathrm{TNF}}$ | | | * | $h_{6\mathrm{TNF}}$ | | | * |
| $\eta_{8\mathrm{TNF}}$ | | | * | $h_{8\mathrm{TNF}}$ | | | * |
| $\eta_{M10}$ | Half-max of $M_A$, TNF-$\alpha$, IL6 and IL8, resp. regulating IL10 | $pg\ ml^{-1}$ | * | $h_{M10}$ | Exp. modulating $M_A$, TNF-$\alpha$, IL6 and IL8, resp. effect on IL10 | - | * |
| $\eta_{\mathrm{TNF}10}$ | | | * | $h_{\mathrm{TNF}10}$ | | | * |
| $\eta_{610}$ | | | * | $h_{610}$ | | | * |
| $\eta_{810}$ | | | * | $h_{810}$ | | | * |
| $\eta_{\mathrm{TNF}6}$ | Half-max of TNF-$\alpha$, IL6 and IL10, resp. regulating IL6 | $pg\ ml^{-1}$ | * | $h_{\mathrm{TNF}6}$ | Exp. modulating TNF-$\alpha$, IL6 and IL10, resp. effect on IL6 | - | * |
| $\eta_{66}$ | | | * | $h_{66}$ | | | * |
| $\eta_{106}$ | | | * | $h_{106}$ | | | * |
| $M_\infty$ | Max number of monocytes | noc | * | | | | |
| | | | **Cardiovascular submodel** | | | | |
| $R_a$ | Resistance in arteries and veins | $\frac{mmHg\ min}{ml}$ | ‡ | $E_{la}$ | Elastance of large and small arteries and veins | $\frac{mmHg}{ml}$ | ‡ |
| $R_v$ | | | ‡ | $E_{sa}$ | | | ‡ |
| $E_m$ | Min and max elastance | $\frac{mmHg}{ml}$ | * | $E_{lv}$ | | | ‡ |
| $E_M$ | | | ‡ | $E_{sv}$ | | | ‡ |
| | | | **Regulatory submodel** | | | | |
| $k_{T\mathrm{TNF}}$ | Rate of Temp change irt TNF-$\alpha$, IL6 and IL10 | – | * | $\tau_1$ | Temp time constant | $hr^{-1}$ | # |
| $k_{T6}$ | | | # | $k_T$ | Temp rate of change | - | * |
| $k_{T10}$ | | | * | $T_b$ | Baseline and max Temp | °C | ‡ |
| $\eta_{T\mathrm{TNF}}$ | Half-max of TNF-, IL6 and IL10, resp. regulating Temp | $pg\ ml^{-1}$ | * | $T_M$ | | | * |
| $\eta_{T6}$ | | | * | | | | |
| $\eta_{T10}$ | | | * | | | | |
| $h_{T\mathrm{TNF}}$ | Exp. modulating TNF-$\alpha$, IL6 and IL10, resp. effect on Temp | – | * | $k_{\mathrm{PT}}$ | PT rate of change | $h^{-1}$ | # |
| $h_{T6}$ | | | * | $k_{\mathrm{PT}E}$ | Rate of PT change in response to endotoxin | $\frac{kg}{hr\ ng}$ | # |

(*Continued*)

**Table 1. Continued**

| Par. | Description | Unit | | Par. | Description | Unit | |
|---|---|---|---|---|---|---|---|
| $h_{T10}$ | | | * | $PT_b$ | Baseline PT | kPa | ‡ |
| $k_{NM}$ | $M_A$ production rate of NO | $(\text{hr noc})^{-1}$ | * | $k_N$ | NO decay rate | $\text{hr}^{-1}$ | * |
| $\eta_{NTNF}$ | Half-max of TNF-$\alpha$ and IL10, resp. regulating NO | $\text{pg ml}^{-1}$ | * | $h_{NTNF}$ | Exp. modulating TNF-$\alpha$ and IL10, resp. effect on NO | - | * |
| $\eta_{N10}$ | | | * | $h_{N10}$ | | | * |
| $k_{RPT}$ | Rate of $R_s$ change in response to PT and NO | $\frac{\text{mmHg min}}{\text{ml hr}}$ | # | $\eta_{RPT}$ | Half-max of PT regulating $R_s$ | kPa | * |
| $k_{RN}$ | | | ** | $R_b$ | Baseline $R_s$ | $\frac{\text{mmHg min}}{\text{ml}}$ | # |
| $k_R$ | $R_s$ decay rate | $\text{hr}^{-1}$ | # | | | | |
| $\eta_{HT}$ | Half-max of Temp regulating HR | °C | ** | $\tau_2$ | HR time constant | $\text{hr}^{-1}$ | ** |
| $\eta_{HP}$ | Half-max of BP regulating HR | $\text{beats min}^{-1}$ | * | $k_H$ | HR rate of change | – | # |
| $h_{HT}$ | Exp. modulating Temp and BP, resp. effect on HR | – | * | $H_b$ | Baseline and max HR | $\text{beats min}^{-1}$ | ‡ |
| $h_{HP}$ | | | * | $H_M$ | | | ‡ |
| $BP_b$ | Baseline BP | mmHg | ‡ | | | | |

*Population. **Manually tuned subject-specific. #Estimated subject-specific. ‡ Derived from data subject-specific.

($w_{\text{TNF}}$, $w_{\text{IL6}}$, $w_{\text{IL8}}$, $w_{\text{IL10}}$). The remaining values are from our previous model (Brady *et al.* 2018).

*Cardiovascular submodel.* We calculate the cardiovascular parameters as described by Brady (2017). The values for elastance in each compartment ($El_i$) and minimum and maximum elastance ($El_m$ and $El_M$), are computed with the equations

$$El_i = \frac{p_i}{V_{st,i}}\ , \quad V_{\text{st},i} = V_i - V_{\text{un},i},\ El_m = \frac{\text{p}_{\text{lv}}}{V_{\text{ED}}},$$
$$El_M = \frac{p_{\text{la}}}{V_{\text{ES}}}, \tag{11}$$

where $V_{\text{st},i}$ (mL) is the stressed volume and $V_{\text{un},i}$ (mL) is the unstressed volume in compartment $i$. The stressed end-diastolic ($V_{\text{ED}} = 132$ mL) and end-systolic ($V_{\text{ES}} = 37$ mL) volume are consistent with values for a healthy individual (Hudsmith *et al.* 2005).

The calculation of $V_{\text{st},i}$ assumes that systemic volume is 85% of total blood volume, whereas the arterial and venous volumes are 20% and 80% of systemic volume, respectively (Brady, 2017). Total blood volume [$V_{\text{tot}}$ (mL)] is a function of body surface area $BSA$ (cm$^2$), height $h$ (cm), weight $w$ (kg) and gender given by

$$V_{\text{tot,female}} = 1000\,(3.47\text{BSA} - 1.954)\,,$$
$$V_{\text{tot,male}} = 1000\,(3.29\text{BSA} - 1.229)\,,$$
$$BSA = \sqrt{\frac{h\,w}{3600}}.$$

*Cardiovascular control submodel.* Parameter values are adapted from Brady (2017) and adjusted where necessary to align with the data. We set the parameters representing the baseline levels of temperature, HR, and SBP ($T_b$, $H_b$ and $BP_b$, respectively) to the initial points in the data. The equations for temperature and HR also have maximum level parameters ($T_M$ and $H_M$, respectively) informed by the literature. $T_M$ is 39.5 °C is the cut-off for life-threatening hyperthermia (Roti Roti, 2008). Maximum HR is calculated by

$$H_M = 207 - 0.7\text{Age},$$

where $H_M$ is measured in beats min$^{-1}$ and Age is measured in years (Gellish *et al.* 2007). In addition, the delay $\kappa$ is chosen to ensure that NO increases 2 to 4 hr after LPS administration (Kirkebøen & Strand, 1999).

**Parameter estimation.** We fit the model to the measurements for immune mediators, temperature, SBP and HR by minimizing the least squares error

$$J = r^T\, r,\ \text{where}\ r = \frac{1}{\sqrt{N}}\left(\frac{Y_{\text{model}} - Y_{\text{data}}}{\overline{Y_{\text{data}}}}\right), \tag{12}$$

where $Y_{\text{model}}$ and $Y_{\text{data}}$ are the model output and measured data, respectively. $\overline{Y_{\text{data}}}$ is the mean of the data and $N$ is the total number of data points (Mathews & Fink, 2004). The cost function $J$ is minimized using built-in optimization

**Table 2. Nominal parameter (Par) values**

| Population | | | | Patient-specific | | | |
|---|---|---|---|---|---|---|---|
| Par. | Value | Par. | Value | Par. | Mean ± SD | Par. | Mean ± SD |
| $k_M$ | 0.0414 | $h_{66}$ | 1.00 | $k_E$ | 0.967 ± 0.131 | $E_{la}$ | 0.724 ± 0.077 |
| $k_{M\mathrm{TNF}}$ | $4.14\times10^{-6}$ | $h_{106}$ | 3.68 | $k_{\mathrm{TNF}M}$ | 0.678 ± 0.208 | $E_{sa}$ | 3.90 ± 0.41 |
| $k_{6\mathrm{TNF}}$ | 0.813 | $E_m$ | 0.0265 | $k_{6M}$ | 0.813 ± 0.319 | $E_{lv}$ | 0.113 ± 0.011 |
| $k_{8\mathrm{TNF}}$ | 0.56 | $k_{T\mathrm{TNF}}$ | 1.50 | $k_{8M}$ | 0.515 ± 0.109 | $E_{sv}$ | 0.0213 ± 0.0022 |
| $k_{106}$ | 0.0191 | $k_{T6}$ | 1.50 | $k_{10M}$ | 0.0158 ± 0.005 | $T_b$ | 36.8 ± 0.4 |
| $\eta_{ME}$ | 3.30 | $k_{T10}$ | 0.0625 | $k_{\mathrm{TNF}}$ | 1.03 ± 0.165 | $\mathrm{PT}_b$ | 714 ± 268 |
| $\eta_{M\mathrm{TNF}}$ | 100 | $\eta_{T\mathrm{TNF}}$ | 185 | $k_6$ | 0.642 ± 0.0867 | $k_{\mathrm{RPT}}$ | 26.8 ± 19.1 |
| $\eta_{6\mathrm{TNF}}$ | 185 | $\eta_{T6}$ | 560 | $k_8$ | 0.700 ± 0.175 | $k_{RN}$ | 1.10 ± 0.99 |
| $\eta_{8\mathrm{TNF}}$ | 185 | $\eta_{T10}$ | 34.8 | $k_{10}$ | 0.865 ± 0.201 | $k_R$ | 4.64 ± 2.27 |
| $\eta_{M10}$ | 4.35 | $h_{T\mathrm{TNF}}$ | 0.75 | $w_{\mathrm{TNF}}$ | 1.12 ± 0.26 | $R_b$ | 1.22 ± 0.13 |
| $\eta_{\mathrm{TNF}10}$ | 17.4 | $h_{T6}$ | 0.75 | $w_{\mathrm{IL6}}$ | 1.05 ± 0.52 | $\eta_{HT}$ | 36.3 ± 0.4 |
| $\eta_{610}$ | 34.8 | $h_{T10}$ | 1.00 | $w_{\mathrm{IL8}}$ | 3.01 ± 0.77 | $BP_b$ | 118 ± 8 |
| $\eta_{810}$ | 17.4 | $\tau_1$ | 1.00 | $w_{\mathrm{IL10}}$ | 0.235 ± 0.161 | $\tau_2$ | 0.496 ± 0.287 |
| $\eta_{\mathrm{TNF}6}$ | 560 | $k_T$ | 0.50 | $R_a$ | 0.0665 ± 0.0070 | $k_H$ | 0.269 ± 0.084 |
| $\eta_{66}$ | 560 | $T_M$ | 39.5‡ | $R_v^*$ | 2.90 ± 0.29 | $H_b$ | 60.5 ± 8.9 |
| $\eta_{106}$ | 560 | $k_{\mathrm{PT}}$ | 0.15 | $E_M$ | 3.11 ± 0.26 | $H_M$ | 190 ± 3 |
| $M_\infty$ | $3.00\times10^4$ | $k_{\mathrm{PT}E}$ | 0.20 | | | | |
| $k_{MR}$ | $6.00\times10^{-3}$ | $k_{NM}$ | $2.00\times10^{-3}$ | | | | |
| $k_{MA}$ | 2.51 | $\eta_{N\mathrm{TNF}}$ | 95.0 | | | | |
| $h_{ME}$ | 1.00 | $\eta_{N10}$ | 4.00 | | | | |
| $h_{M\mathrm{TNF}}$ | 3.16 | $k_N$ | 0.045 | | | | |
| $h_{6\mathrm{TNF}}$ | 2.00 | $h_{N\mathrm{TNF}}$ | 2.00 | | | | |
| $h_{8\mathrm{TNF}}$ | 3.00 | $h_{N10}$ | 0.40 | | | | |
| $h_{M10}$ | 0.30 | $\eta_{RPT}$ | 230 | | | | |
| $h_{\mathrm{TNF}10}$ | 3.00 | $h_{RPT}$ | 2.00 | | | | |
| $h_{610}$ | 4.00 | $\eta_{HP}$ | 143 | | | | |
| $h_{810}$ | 1.50 | $h_{HT}$ | 2.00 | | | | |
| $h_{\mathrm{TNF}6}$ | 2.00 | $h_{HP}$ | 4.00 | | | | |

Parameter denoted by a double dagger (‡) was taken from Roti Roti (2008). $*\times10^{-3}$.
Inflammatory submodel was taken from Brady *et al*. (2018). All other parameters (cardiovascular - and regulatory - submodels) were taken from Brady (2017). Colours indicate inflammatory (light grey), cardiovascular (grey) and regulatory (dark grey) submodel parameters.

routines in MATLAB (MathWorks Inc., Natick, MA, USA).

We used sensitivity analysis and subset selection for each subsystem (the inflammatory, regulatory and cardiovascular modules) of our mathematical model to determine which parameters to estimate.

We calculated relative sensitivities $S = \partial r/\partial \log(\theta)$ using forward finite differences with a tolerance $\varphi = \sqrt{10^{-8}}$, applying a local approach where parameters are varied one at a time. If small perturbations in a parameter result in significant changes in the output, the parameter is sensitive. If not, then the parameter is insensitive. We computed the sensitivities from the solution of the ODEs with the nominal parameter values. Ranked sensitivities were computed using the two-norm, averaging the time-varying sensitivities.

To determine a subset of identifiable parameters (Table 3), we used the structured correlation method (Olufsen & Ottesen, 2013) to compute the covariance matrix

$$c_{ij} = \frac{F_{ij}}{\sqrt{F_{ii}F_{jj}}}\ , \quad F_{ij} = \left(S^T S\right)^{-1}.$$

For this calculation, the Fisher information matrix $F$ only includes parameters above the sensitivity threshold. Parameters with a pairwise correlation coefficient $|c_{ij}| > 0.95$ were assumed correlated. For each correlated pair, the least sensitive parameter was excluded from the subset and kept at its nominal value during the optimization. Brady (2017) gives a detailed description of the sensitivity analysis and subset selection.

**Table 3. Optimal population-uniform (UF) and patient-specific (PS) parameter (Par) values for model calibration and validation**

| Par. | Calibration (18 PS pars), mean ± SD | Calibration (6 UF, 12 PS pars), mean ± SD | Validation (Copeland *et al.*, 2005) | Validation (Janum *et al.*, 2016) |
|---|---|---|---|---|
| $k_6$ | 0.905 ± 0.315 | 0.797 | 0.797 | 0.797 |
| $k_8$ | 0.773 ± 0.182 | 0.698 | 0.698 | 0.698 |
| $k_{TNF}$ | 1.09 ± 0.23 | 1.49 | 1.49 | 1.49 |
| $k_{TNFM}$ | 0.593 ± 0.099 | 0.697 | 0.697 | 0.697 |
| $k_E$ | 0.874 ± 0.459 | 1.08 | 1.08 | 1.08 |
| $\tau_1$ | 1.67 ± 0.67 | 1.69 | 1.69 | 1.69 |
| $k_{10}$ | 0.835 ± 0.254 | 0.959 ± 0.712 | 1.11 | 0.623 |
| $k_{10M}$ | 0.023 ± 0.027 | 0.022 ± 0.025 | 0.0205 | 0.0078 |
| $k_{6M}$ | 0.856 ± 0.876 | 0.644 ± 0.558 | 0.988 | 0.511 |
| $k_{8M}$ | 0.895 ± 1.099 | 0.792 ± 0.984 | 0.070 | 0.372 |
| $R_b$ | 1.19 ± 0.18 | 1.27 ± 0.23 | 1.08 | 1.30 |
| $k_{T6}$ | 2.92 ± 1.67 | 2.80 ± 1.56 | 1.88 | 2.67 |
| $k_{PTE}$ | 0.152 ± 0.128 | 0.16 ± 0.11 | 0.160 | 0.179 |
| $k_{RPT}$ | 43.8 ± 61.1 | 32.6 ± 33.6 | 19.8 | 4.89 |
| $k_{RN}^*$ | 1.10 ± 0.99 | 1.10 ± 0.99 | 2.00 | 0.65 |
| $k_R$ | 6.03 ± 3.72 | 4.76 ± 3.99 | 7.15 | 1.85 |
| $\tau_2^*$ | 0.496 ± 0.287 | 0.496 ± 0.287 | 0.200 | 0.500 |
| $k_H$ | 0.262 ± 0.090 | 0.268 ± 0.095 | 0.236 | 0.247 |

Parameters denoted with an asterisk (∗) were tuned manually. Colours indicate inflammatory (light grey), cardiovascular (grey) and regulatory (dark grey) submodel parameters.

**Model calibration and validation.** For each patient in the Janum study, we used built-in MATLAB optimization functions to estimate each submodel's sensitive and identifiable parameters. Next, we calculated the coefficient of variation (CoV) to determine which parameters are population uniform (i.e., the parameters that do not vary significantly between patients). We used nested optimization to find the optimal uniform value allowing the other parameters to vary and evaluated the goodness of fit. We repeated this analysis, computing the CoV, determining if additional parameters are uniform, optimizing and evaluating the fitting power until the goodness of fit decreases. This analysis is performed on each submodel to find uniform and patient-specific parameters. We used optimization to validate the model, estimating parameters that minimize the least-squares error between model predictions and mean data from the Copeland study. For this simulation, we keep the uniform population parameters constant while the patient-specific parameters vary.

## Therapeutic interventions

The Janum and Copeland studies analyse the response to a bolus LPS injection, where the presence of LPS in the circulation is transient, and SBP generally rises slightly and then decreases back toward the nominal level. Here, we use the model to conduct in-silico exploration of several treatments to mitigate the harmful effects of sustained endotoxin (sustained endotoxaemia) when the body cannot effectively clear the endotoxin on its own (Russell, 2006). Janum and Copeland do not examine this pathological case. Sustained endotoxaemia is characterized by an elevated temperature and HR, and a decrease in SBP below the hypotensive limit (below 100 mmHg) (Lepper *et al.* 2002; Victorino *et al.* 2003; Oyetunji *et al.* 2011; Gotts & Matthay, 2016). We simulate sustained endotoxaemia by forcing LPS to remain constant (at 2 ng kg$^{-1}$) over a 12 hr time window.

With the sustained endotoxaemia model, we simulate the effects of treatments, including LPS adsorption, antipyretics and vasopressors, as well as combinations of these, and we assess each intervention's ability to restore haemostasis. For these studies, we introduce treatment after 4 hr of sustained endotoxaemia.

*LPS adsorption* is a therapeutic strategy used to clear endotoxin from the bloodstream through haemoperfusion. This treatment is recommended as early intervention, within the first 6 hr of diagnosis for sepsis patients (Yaroustovsky *et al.* 2018). To capture the action of LPS adsorption, we increased the decay rate of LPS ($k_E$).

*Antipyretic* treatment, initiated at onset of fever, reduces pain sensitivity and body temperature, helping the body to return to baseline levels faster. This medication is usually

**Table 4. Effects of simulated treatments analyzing the dynamic response to sustained endotoxaemia, LPS adsorption, antipyretics and vasopressors over a 12 h time span**

| Pathological input | Response |
|---|---|
| Transient endotoxaemia | Slight $M_R$ decrease and $M_A$ increase. Cytokine levels increase, reach a peak and fall back to nominal levels. Temperature rises to a febrile level and decreases back to baseline. HR increases then starts to return toward baseline. Slight increase in BP followed by a decrease toward nominal level. PT exhibits a small decrease and returns toward baseline. Elevated NO |
| Sustained endotoxaemia | Pronounced $M_R$ decrease and $M_A$ increase. Pro-inflammatory cytokines reach a peak earlier. Max concentration is similar to transient case. Slow increase occurs toward the end of the 12-h window. IL-10 reaches a much larger peak. Fever occurs, and temperature does not return to baseline. HR level increases and stays significantly high. Initial increase in BP followed by a decrease to a hypotensive level. Significantly elevated NO and notable PT decline |
| | **Intervention** |
| LPS adsorption | Temperature and HR are brought down toward nominal levels. A recovery also occurs in the PT |
| Antipyretics | Improvement in temperature and PT in the time windows of greatest action (4-7 h and 10–12 h). Slight increase in temperature and decrease in PT in the period 7–10 h due to a delayed effect of second dose. HR decreases but does not recover to nominal level. Same cytokine and NO levels as in **Sustained endotoxaemia** |
| Vasopressors | Increase in resistance, which translates into recovery of BP to its nominal level. HR remains elevated. NO, PT, temperature and cytokine responses are the same as in **Sustained endotoxaemia** |
| LPS adsorption and Antipyretics | Temperature, HR and PT return toward their baseline levels |
| LPS adsorption and Vasopressors | Recovery in temperature, HR, BP and PT. The decrease in HR and temperature is noticeably slower compared to the **LPS adsorption and antipyretics** treatment |
| Antipyretics and Vasopressors | Temperature, HR, BP and PT return toward nominal levels, but the recovery is noticeably slower compared to the **LPS adsorption and vasopressors** intervention |
| All three interventions | Pain alleviation and recovery of normal body temperature, HR and BP are achieved in the shortest amount of time |

Simulations are conducted changing endotoxin (LPS stimulus) and imposing treatments for each patient in the study by Janum *et al*. (2016). Prediction results from a representative subject are shown in Figs 8 and 9, and characteristic patient variation in simulations is plotted on Fig. 10.

administered every 6 hr (Niven *et al*. 2013) and takes effect with a delay of about 3 hr (Plaisance & Mackowiak, 2000). We model this treatment by modifying the equations for PT and temperature to allow for a faster recovery.

*Vasopressors* are used to counteract the significant drop in BP, resulting from the inflammatory response to sustained endotoxaemia (Russell, 2006; Rudiger & Singer, 2013; Gotts & Matthay, 2016). We model vasopressor treatment by increasing the rate at which vascular resistance approaches its baseline level, which in turn affects BP.

*Combination treatments*. In addition to examining the subject-specific effects of LPS adsorption, antipyretics and vasopressors, we combine two interventions, and a therapeutic protocol using all three interventions. The motivation for a multimodal treatment is to target LPS, pain, fever and resistance simultaneously. A detailed description of our implementation of the therapeutic strategies is provided in the Appendix.

## Results

### Data

The immune and physiological markers (marked with blue points on Figs 5 and 6) in both studies exhibit similar behaviour, although there are also several differences. Figure 5 shows the response for two characteristic subjects and Fig. 6 shows the mean ± SD response for the population. From these figures, we observe thefollowing dynamics: Temperature increases in response to the LPS challenge; it reaches a peak between 3 and 4 hr, followed by recovery to baseline. SBP increases, reaching a peak close to 1.5 hr, and then decreases toward the base level. Heart rate shows a significant increase in response to LPS 3–4 hr after the injection. It should be noted that the Janum study only reports HR for 6 hr post LPS injection, whereas the Copeland study (compare Fig. 6A and 6B) reports HR measurements for 9 hr. To compare datasets, for both studies, we only used data from 0–6 hr.

The pro-inflammatory cytokines TNF-$\alpha$, IL-6 and IL-8 reach peak concentrations close to 2 hr after the LPS administration and then return toward baseline. The peak IL-8 concentrations measured for subjects in the Janum study are noticeably higher than the value reported in the Copeland study. The anti-inflammatory cytokine IL-10 reaches its highest level close to 3 hr in the Janum study, whereas Copeland does not measure IL-10.

## Model calibration and validation

We calibrated the model to individual patient data from the Janum study and validated the model against the Copeland data. We used the coefficient of variation (CoV) to identify parameters that are uniform across all patients. Figure 7 shows the parameter distributions for the nine parameters of the inflammatory submodel. $k_{\mathrm{TNF}M}$ is shown to have the least variation between patients. We used nested optimization to find the uniform value for $k_{\mathrm{TNF}M}$ and the patient-specific values for the remaining eight parameters. The goodness of fit ($R^2$) was computed for these values. This process was repeated iteratively until the overall $R^2$ value decreased, and the CoV could no longer be decreased. We repeated this process for each submodel and found six uniform parameters and 12 patient-specific parameters. Model fit comparisons for two patients estimating the 18 patient-specific parameters *vs*. fits with six uniform and estimating 12 patient-specific parameters are shown in Fig. 5 (comparisons for all patients are included in the Supporting information (Doc. S1, Figs. S1-S20). The results show that the reduced model

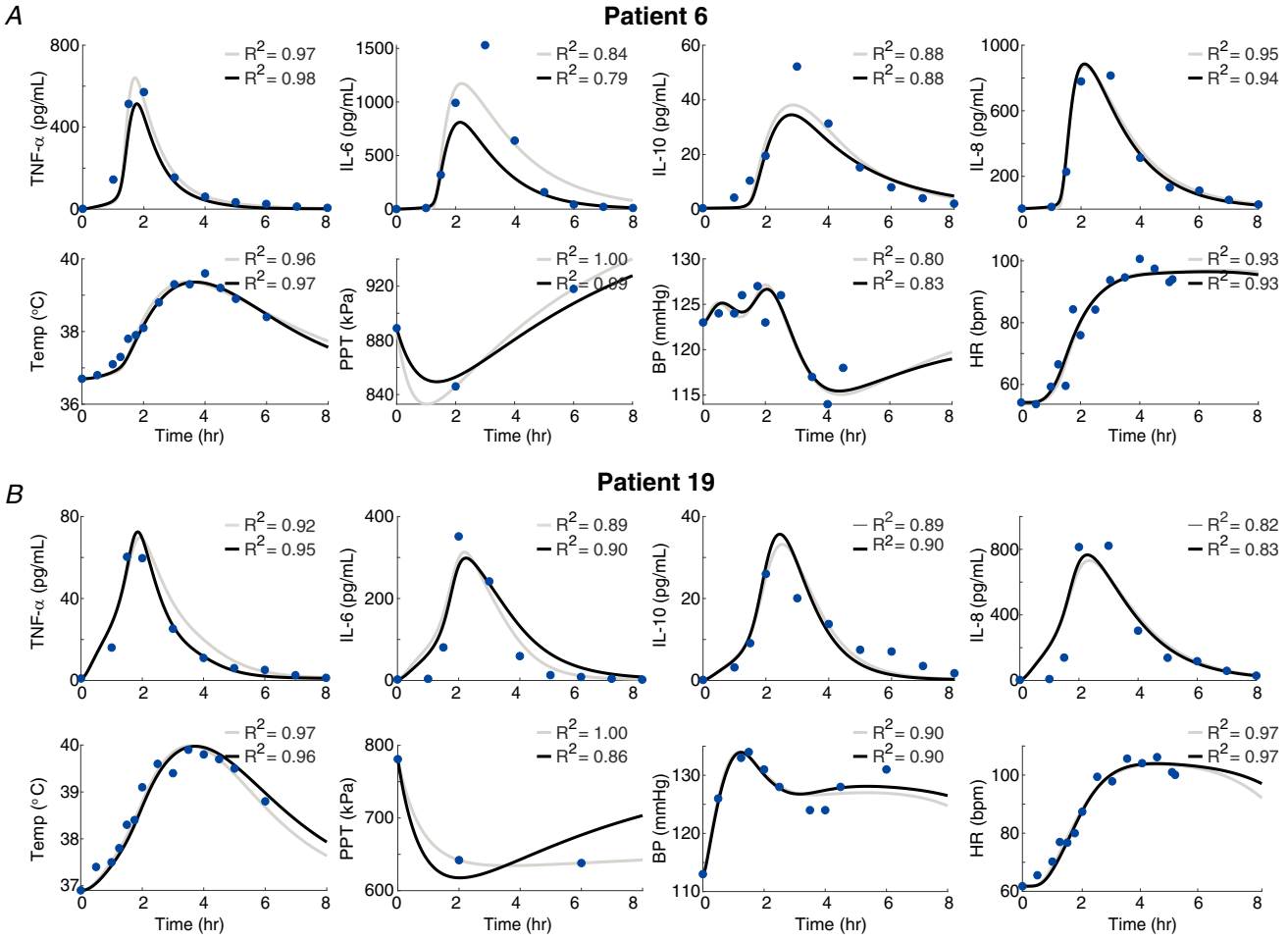


**Figure 5. Model calibration**
Model calibration comparison for two representative patients, 6 (*A*) and 19 (*B*), from the study by Janum *et al*. (2016). For each patient, we compare the results estimating 18 (identifiable and sensitive) patient-specific parameters (grey lines) and predictions with six population-uniform parameters and estimating 12 patient-specific parameters (black lines). The black curves show that, despite fewer patient-specific parameters, the model is able to fit the data equally well for both patients. Mean ± SD values for the estimated parameters are given in Table 3 and values for parameters not estimated are reported in Table 2. Finally, values for all individual subjects are provided in the Supporting information (Doc. S1, Figures S1-S20).

can fit the data equally well despite having fewer degrees of freedom (the mean $R^2$ values over all subjects in the Janum study for inflammatory markers, temperature, pain, BP and HR are: 0.81, 0.90, 0.87, 0.65 and 0.89, respectively). Table 3 lists the uniform parameters and the mean ± SD for the patient-specific parameters. Parameter values for each subject are included in the Supporting information (Doc. S1, Tables S1 and S2).

Figure 5 shows that the model captures key features exhibited in the data: increased pro-inflammatory activity in response to LPS increases body temperature, HR, pain perception and BP. The pro-inflammatory cytokines TNF-$\alpha$, IL-6 and IL-8 increase ∼1 hr following the LPS injection, reach a peak concentration at ∼2 hr and return toward their baseline levels at ∼4 hr. IL-10 rises shortly after the other cytokines, close to 1.5 hr post endotoxin administration. IL-10 reaches its maximum between 2.5 and 3 hr, causing the pro-inflammatory cytokines to decrease. The inflammatory cascade induced by LPS, resulting in elevated TNF-$\alpha$ and IL-6 concentrations, increases HR and core body temperature (to a febrile level) in 3.5–4 hr. As the PT falls (increasing pain perception), BP rises slightly, reaching a peak at ∼1.5 hr.

Figure 6 shows our model validation results for the average Copeland data (Fig. 6A) and the average Janum data (Fig. 6B) estimating 12 patient-specific parameters, using the six uniform population parameters found during model calibration. This figure demonstrates that the model can fit the data with high accuracy. The $R^2$ values for temperature, BP and HR, and the average $R^2$ value for inflammatory markers are 0.99, 0.92, 0.99 and 96, respectively, for the Copeland data, and 0.99, 0.78, 0.98 and 0.95, respectively, for the Janum data. The estimated patient-specific parameters are listed in Table 3.

## Therapeutic interventions

In addition to fitting the model to data, we used simulation to explore the responses of temperature, pain, HR and SBP to different treatment modalities, including LPS adsorption, antipyretics and vasopressors, as well as

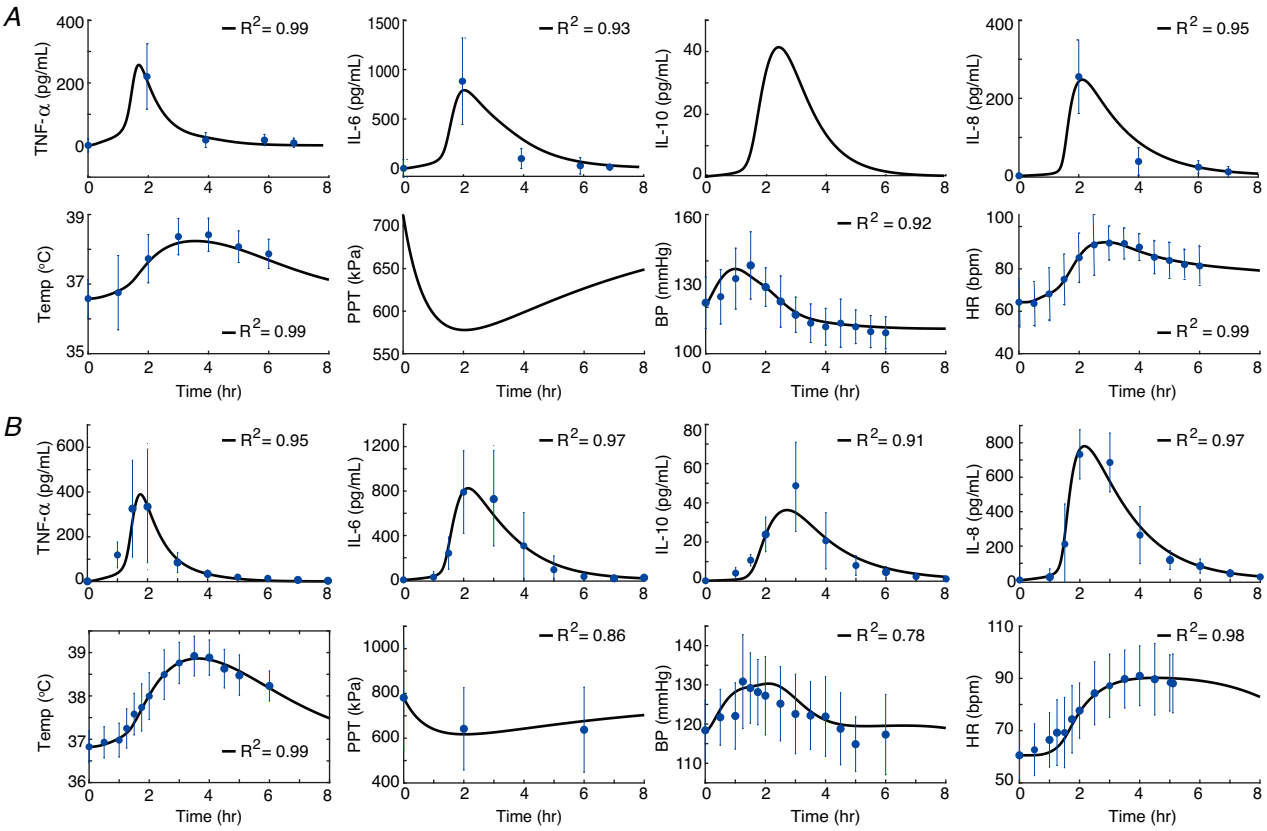


**Figure 6. Model validation**
Model fits to mean data from the studies by Copeland *et al*. (2005) (*A*) and Janum *et al*. (2016) (*B*) using the six population-uniform parameter values found in the calibration step and estimating 12 patient-specific parameters. The parameter values for these simulations are listed in Table 3. The data from Copeland *et al*. (2005) were digitized from Figure 4, which includes error bars for the SEM. We multiplied the digitized SEM by the square root of the sample size ($n = 10$) to obtain the standard deviation plotted here.

combinations of these. The effects of treatments are compared with the response to sustained endotoxaemia. We introduce treatments after 4 hr of sustained endotoxaemia, and we define the efficacy of interventions as the ability to return all physiological signals to their baseline levels in the shortest time. Below, we describe general response exhibited in 10 or more subjects (summary in Table 4). We ran simulations with treatments for each patient, using the 18 estimated patient-specific parameters. The results for a characteristic subject are summarized in Figs 8 and 9, and characteristic variations observed in treatments are summarized in Fig. 10. Simulations for each subject are included in the Supporting information, Doc. S1, Figures S21-S40.

*Transient endotoxaemia* (base case – grey lines in Figs 8 and 9) is induced via stimulation of the immune system by a low bolus dose (2 ng $kg^{-1}$) of LPS. In response, monocytes are activated, increasing both pro- and anti-inflammatory cytokines. The latter leads to increases in NO, body temperature (to a febrile level), HR and SBP. Also, the body becomes more sensitive to pain. Within 12 hr, all physiological signals return to nominal levels.

*Sustained endotoxaemia* (black lines in Figs 8 and 9) is simulated by forcing LPS to remain constant (at 2 ng $kg^{-1}$) over a 12 hr window. This condition significantly increases the number of activated monocytes compared to transient endotoxaemia. In response, the cytokines peak earlier and reach higher maximum concentrations. Most notable is the increase in the anti-inflammatory cytokine IL-10. The immune mediators also exhibit a secondary activation between 4 and 8 hr, resulting in prolonged elevation of body temperature as a result of the slow decay of pyrogens. The significantly higher initial peak in IL-10 translates to a slightly lower peak in temperature because IL-10 suppresses the thermal response. The sustained presence of endotoxin also causes a significant drop in the PT. NO is higher as a result of the release from the increased number of activated monocytes. These response indicators have opposite effects on resistance. The initial change in PT is more dramatic than the increase in NO, resulting in a more significant resistance increase. After 4 hr, the PT decline rate is slow, whereas NO is still elevated, resulting in a lower resistance. The initial rise in resistance leads to an initial increase in SBP and, as the resistance drops, SBP decreases significantly, falling to a hypotensive level, which persists. HR significantly increases as body temperature rises. As the thermal response subsides, HR begins to decrease. However, as SBP falls into the hypotensive range, HR increases again because of the activation of compensatory cardiac acceleration (Hall, 2015).

Figure 10*A* compares BP variations for three subjects. Most subjects in this group experience hypotension (solid black line), followed by a slow recovery, some experience a short duration of hypertension followed by spontaneous

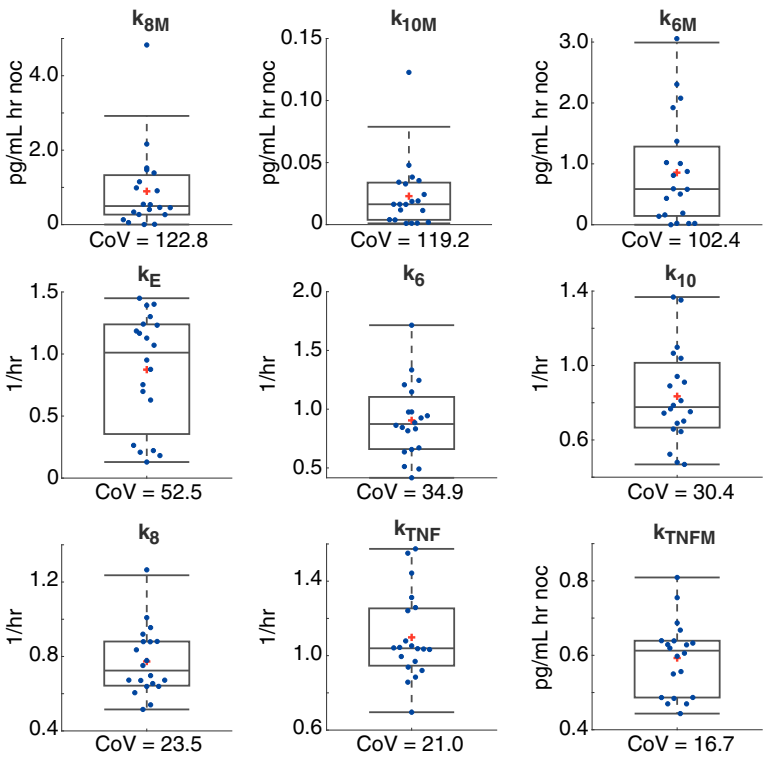


**Figure 7. Inflammatory submodel calibration**
Parameter distributions of the sensitive and identifiable parameters of the inflammatory submodel after fitting submodel to data from 20 patients from the study by Janum *et al*. (2016). Coefficient of variation (CoV) was used to identify parameters that could be uniform between all patients and those that needed to be patient-specific. Boxplots show median including the 25th and 75th percentiles. Parameters are arranged in order of decreasing CoV.

recovery (dashed black line) and a few experienced pronounced hypertension followed by recovery (dotted black line).

*LPS adsorption* (blue lines in Fig. 8), simulated by increasing the LPS decay rate and accelerating the clearance of endotoxin, prevents the secondary immune activation. In response, the immune signals decay faster, promoting fast recovery of the PT, temperature and HR.

*Antipyretics* (red lines in Fig. 8) are simulated by letting the PT and temperature recover faster. The result is a decrease in temperature and increase in the PT. Accounting for the ∼3 hr delay in their therapeutic activity, we simulate the effects of administering

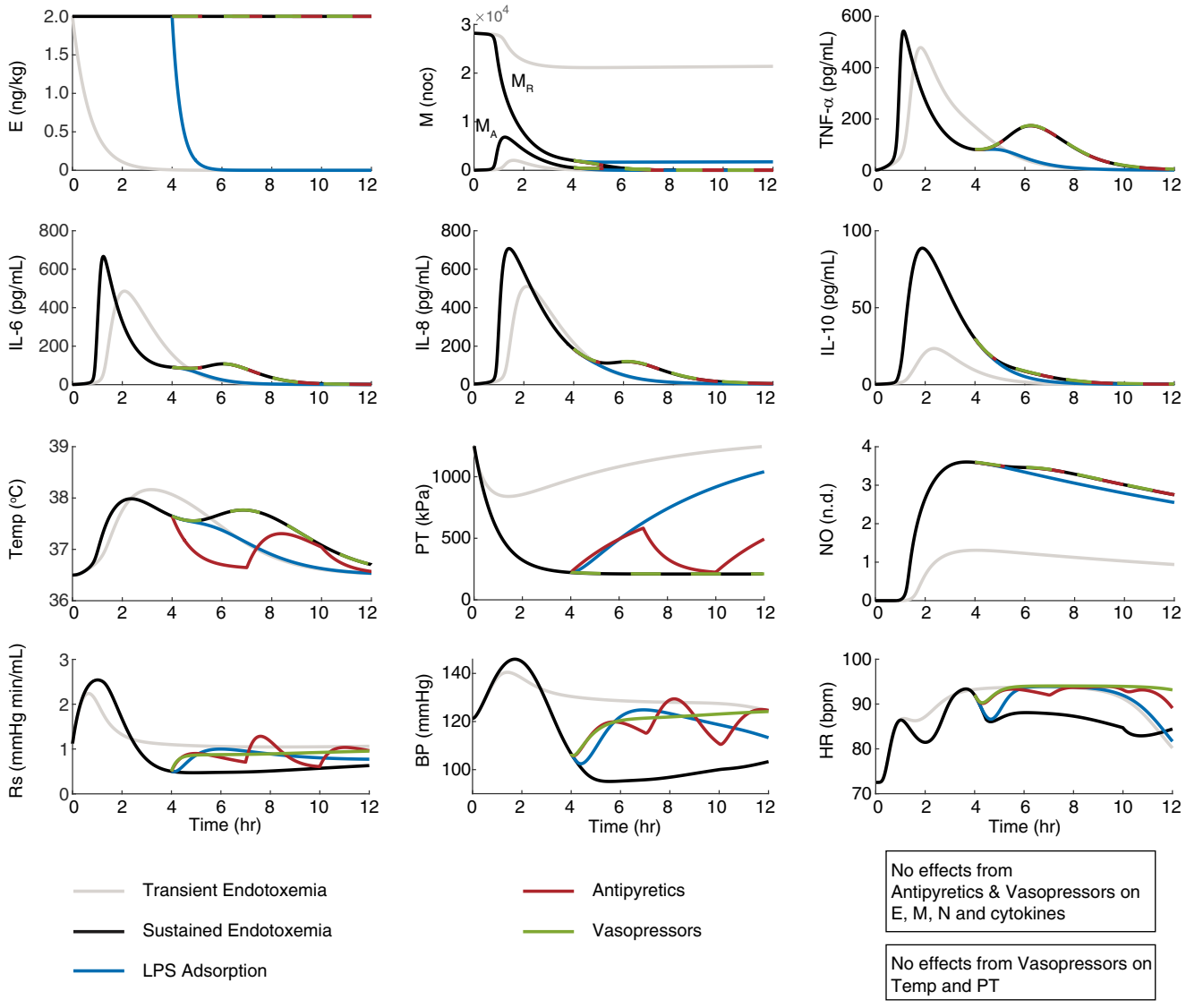


**Figure 8. Model predictions for effects of LPS adsorption, antipyretics and vasopressors on cardio-inflammatory response**

Transient endotoxaemia (grey) serves as the reference baseline. Following sustained presence of endotoxin (E, ng kg$^{-1}$), interventions were induced at $t = 4$ hr. Sustained endotoxaemia (black) induces a decrease in resting (MR, noc) and an increase in the activated (MA, noc) monocytes. In response, temperature (Temp, °C), heart rate (HR, beats min$^{-1}$) and NO (NO, nondimensional) increase, and the pain perception threshold (PT, kPa) decreases. Vascular resistance (Rs, mmHg min mL$^{-1}$) initially increases, resulting in an initial increase in blood pressure (BP, mmHg). Then, BP drops to the hypotensive range. LPS adsorption (blue) results in endotoxin clearance, pain relief (increase in PT), fever reduction and HR normalization. Antipyretics (red) do not affect the endotoxin. Although antipyretics induce some pain relief and decrease fever and HR, they are unable to counteract hypotension. Vasopressors (green) also do not affect the endotoxin. Even though vasopressors do not alleviate fever, pain or abnormally high HR, they are able to normalize BP. Dashes indicate parts where the curves overlap. The response for each individual subject is included in the Supporting information (Doc. S1, Figures S21-S40).

antipyretics at time $t = 1$ hr and $t = 7$ hr by reducing the rate at which endotoxin lowers PT, and the rates at which TNF-$\alpha$ and IL-6 upregulate body temperature by 90% for $4 < t < 7$ hr and $10 < t < 12$ hr. The results show that there is a slight increase in temperature and decrease in PT for $7 < t < 10$ hr as a result of the delay in the second dose taking effect. Although antipyretics lower HR, they do not lower it to the baseline level. Because antipyretics do not directly affect endotoxin levels, the inflammatory mediators and NO remain elevated as in the case of sustained endotoxaemia.

*Vasopressors* (green lines in Fig. 8), similar to antipyretics, do not affect the endotoxin level, and therefore the inflammatory mediators, NO, PT or temperature do not change from the behaviour seen in sustained endotoxaemia. Vasopressors increase vascular resistance, increasing SBP to its nominal level. However, this treatment has little effect on HR.

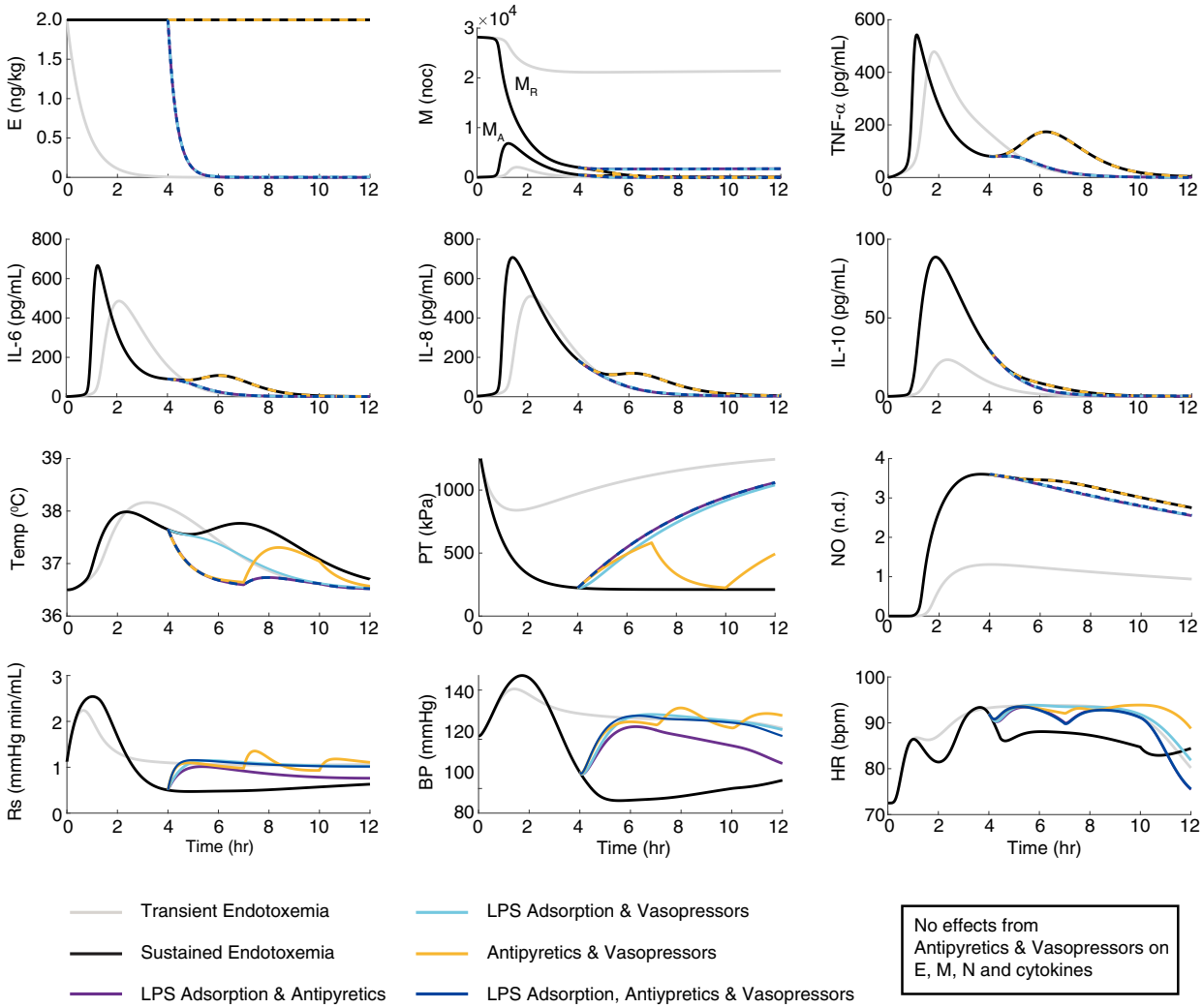


**Figure 9. Model predictions for effects of multimodal treatments on cardio-inflammatory response**
Transient endotoxaemia is shown in grey and sustained endotoxaemia in black. All treatments for sustained endotoxaemia are introduced at $t = 4$ hr. The combinations of therapies perform better compared to individually administered treatments. The LPS adsorption and antipyretics combination (purple) returns temperature (Temp, °C), heart rate (HR, beats min$^{-1}$) and the pain threshold (PT, kPA) toward their baseline levels. LPS adsorption and vasopressors (light blue) reduce pain and help temperature, HR and blood pressure (BP, mmHg) to recover, although, with this therapeutic combination, the decrease in HR and temperature is slower than with LPS adsorption and antipyretics. The combination of antipyretics and vasopressors (yellow) improves the levels of PT, temperature, HR and BP, although the recovery takes place more slowly compared to the case of LPS adsorption and vasopressors. The most effective multimodal treatment is LPS adsorption, antipyretics and vasopressors (dark blue) because all physiological signals recover in the shortest time. Dashes indicate parts where the curves overlap. The response for each individual subject is included in the Supporting information (Doc. S1, Figures S21-S40).

*LPS adsorption and antipyretics* (purple lines in Fig. 9) target endotoxin clearance, pain and fever. This combination promotes fast return of temperature, HR and PT to baseline levels. The improvements occur in a shorter time compared to the individual treatments.

*LPS adsorption and vasopressors* (light blue lines in Fig. 9) act on endotoxin and vascular resistance. Their concurrent administration drives PT toward the base level and leads to recovery in temperature, HR and SBP. However, the decrease in HR and temperature is slower compared to the *LPS adsorption and antipyretics* treatment.

*Antipyretics and vasopressors* (yellow lines in Fig. 9) impact pain, fever and vascular resistance. This combination allows PT, temperature, HR and SBP to approach their baseline levels, although the recovery occurs slower than *LPS adsorption and vasopressors*.

*LPS adsorption*, *antipyretics and vasopressors* (dark blue lines in Fig. 9) target endotoxin clearance, pain, fever and vascular resistance. This treatment regimen alleviates pain and recovers body temperature, HR and SBP in the shortest amount of time.

*Summary*: The intervention strategies gave similar results for most subjects in the population, with the temperature, pain, HR and SBP responses exhibiting similar trends in 10 or more subjects. Figure 10*B–D* summarizes the main variations for characteristic subjects. *LPS adsorption* (Fig. 10*B*). In subjects experiencing hypotension in response to sustained endotoxaemia, the treatment does not initiate SBP recovery toward baseline. Subjects becoming hypertensive do not benefit from this treatment either (dashed and dotted lines) and their SBP does not recover faster with treatment than without. Moreover, patients who become severely hypertensive (SB$P > 160$ mmHg, dotted lines) do not recover within the 12 hr window. *Antipyretics* (Fig. 10*C*). This treatment is ineffective for patients with a severe hypotensive drop (solid lines). For patients experiencing moderate hypotension (dashed lines) or hypertension (dotted lines), the treatment brings BP towards baseline, although the repeated dose may negatively impact recovery. *LPS adsorption and antipyretics* (Fig. 10*D*). Similar to *Antipyretics* alone, patients experiencing large BP decrease (solid lines) do not benefit from this treatment. However, this treatment benefits patients with moderate hypotension (dashed line) and hypertension (dotted line), and they recover faster.

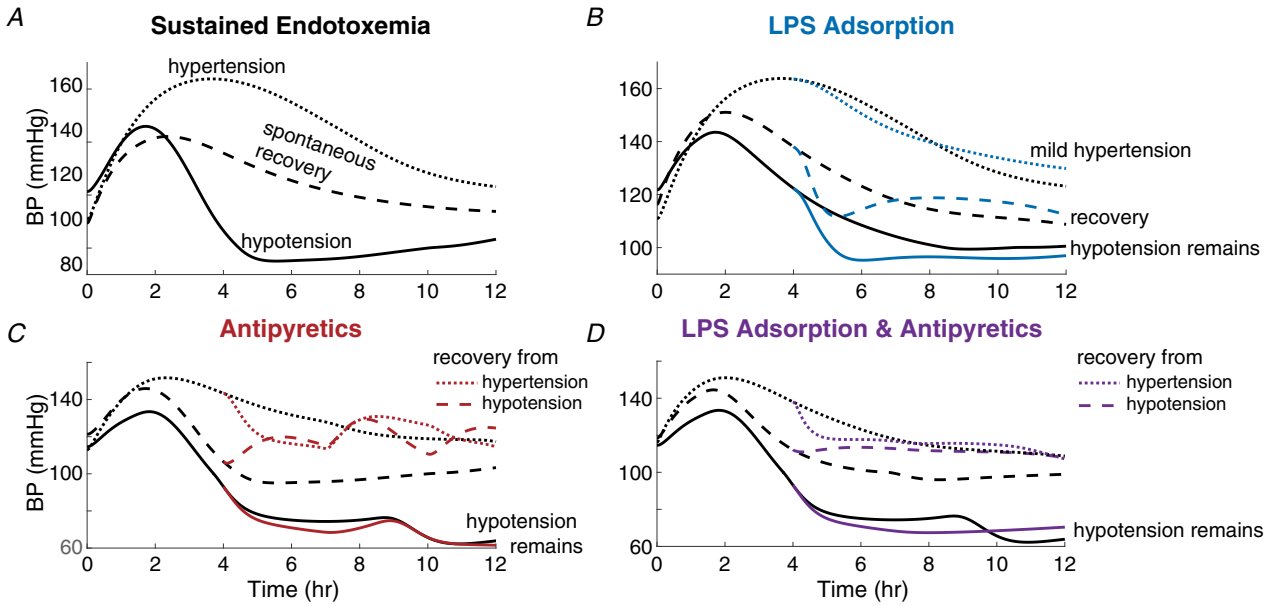


**Figure 10. Characteristic SBP variations in response to treatments**
The results are reported for three characteristic subjects noted by a solid, dashed and dotted line. *A*, the response to sustained endotoxaemia simulated by inducing LPS for 12 hr. The majority of the subjects experience hypotension (solid black line), some experience pronounced hypertension (SBP> 160 mmHg, black dotted line) and some experience spontaneous recovery (black dashed line). The SBP returns to baseline for all subjects, but not all within the 12 hr window. *B–D*, the response to LPS adsorption (blue) and antipyretics (red), as well as the combination of these two treatments (purple), for three characteristic subjects (solid, dashed and dotted). The black lines show the response to sustained endotoxaemia and the coloured lines the response to the treatment. Treatments are considered effective if SBP returns to baseline faster than in sustained endotoxaemia; for example, for patients experiencing moderate hypertension in response to sustained endotoxaemia (dashed lines in *D*), treatment with LPS adsorption and antipyretics is effective because the dashed purple line returns to the base value faster than the dashed black line.

## Discussion

The model developed in this work successfully captures the immune, pain, thermal and cardiovascular behaviour observed in data from two experimental studies of healthy adults given a single LPS injection. The calibration and validation results show that an inflammatory reaction to transient endotoxaemia is associated with fever and elevated HR, pain perception and SBP. Using the model, we were able to estimate dynamics in 20 individual patients, and the model was able to capture patient-specific variation often observed in response to inflammation. In agreement with trends in the data, the model shows that, as the immune response subsides, the physiological signals approach their nominal levels. Similar to previous studies, we account for the cardiovascular implications of immune-mediated NO synthesis, namely vasodilatation. Our model is the first to reflect the dynamics of pain and temperature during an endotoxin challenge.

The pain model describes the interactions between inflammation and systemic vascular resistance, leading to an increased BP via vasoconstriction. The thermal component allowed for capturing the immune system's interaction with HR through the febrile response. Furthermore, the simulation of sustained endotoxaemia shows that, in the presence of fever, when SBP drops significantly, rapid HR has a diminished ability to compensate for hypotension. The latter suggests that the thermal response is important to explain the interaction between BP and HR during an endotoxin challenge, on a time scale of hours.

A sustained presence of endotoxin prompts a cascade of physiological processes acting on multiple timescales, complicating critical care for the patient. We model this pathological state by keeping the LPS level constant, simulating the body's inability to effectively clear LPS from the bloodstream (Russell, 2006). The model predicts detrimental pathophysiological effects, including fever, increased sensitivity to pain, hypotension and elevated HR, which do not resolve spontaneously in most subjects. These results are consistent with the symptoms observed in sepsis (Nguyen *et al*. 2006). However, it should be noted that, in septic patients with Gram-negative infection, the LPS level is much higher than the 2 ng $kg^{-1}$ dose used in the experimental studies from which we obtained calibration and validation data. A mechanism via NO is probably at play when recuperation from hypotension is not successful. As the number of activated monocytes expands, the concentration of NO becomes sufficiently elevated to exert a more substantial vasodilatory impact on peripheral vascular resistance than the vasoconstrictive effect of changes in PT.

Our simulation results also show some qualitative deviations from the trend of hypotension in response to sustained endotoxaemia. These include light hypertension followed by spontaneous recovery and pronounced hypertension, subsequently followed by SBP decrease to a mildly hypertensive level (Fig. 10). When spontaneous recovery occurs, the immune dynamics differ only slightly compared to transient endotoxaemia and, consequently, the NO increase is not enough to produce pronounced vasodilatation and hypotension. The latter can be interpreted as higher resistance to endotoxin.

For hypertensive patients, the change in the PT is dramatic, leading to a notable increase in SBP, with the NO increase and subsequent vasodilatation being insufficient to balance this effect. The qualitative variations in SBP behaviour could be attributed to differences in immune and pain responses. Compared to hypertension, hypotension is associated with higher levels of monocyte activation and TNF-$\alpha$, and a lower IL-10 concentration, which are factors driving pronounced vasodilatation via a significant rise in NO. Moreover, during hypotension, changes in the PT occur more slowly than the hypertension case.

We perform *in silico* investigations to explore the impact of interventions used in the clinical management of endotoxaemia: LPS adsorption, vasopressors and antipyretics. LPS adsorption is a therapy for reducing the endotoxin load (Yaroustovsky *et al*. 2018). Our simulation results show that this treatment leads to HR normalization and relief of fever and pain. Vasopressor medication targets the cardiovascular system. Our *in silico* analysis demonstrates that vasopressors successfully normalize SBP, but do not alleviate fever, pain and abnormally high HR. Antipyretics are used to reduce core body temperature and pain (Plaisance & Mackowiak, 2000). However, they do not block the dynamics of inflammatory cytokines (Toussaint *et al*. 2010) and their benefits and drawbacks are not well understood (Plaisance & Mackowiak, 2000). Fever may serve an essential role in fighting the infection, although it may also negatively impact the cardiovascular system. Our findings indicate that antipyretics have favourable effects on pain, body temperature, and HR.

LPS adsorption prompts an increase in the PT and recovery of temperature and HR, although hypotension could persist. This treatment is introduced after the number of activated monocytes reaches a peak, and it only slightly lowers the level of NO, so hypotension results when NO-mediated vasodilatation overpowers vasoconstriction. A similar outcome is found with antipyretics because they do not impact the immune dynamics and therefore the NO level.

Other possible outcomes for SBP, as suggested by the simulation results for LPS adsorption, are recovery from hypertension and mild hypertension. In those cases, the NO level is not dramatically increased, and the PT rate of change is large, which contributes to vasoconstriction. Furthermore, with antipyretics, a qualitative variation in SBP behaviour is recovery from hypotension, where

vasodilatation manages to push SBP into the hypotensive range, although the PT change is sufficiently large to pull SBP back up to the baseline level.

Uncontrolled infection, which can spread and lead to sepsis, is multifaceted, with numerous possibilities for treatment, as seen in its pathophysiology and recent treatment guidelines (Hotchkiss & Karl, 2003; Howell & Davis, 2017). Multimodal therapeutic strategies for sustained endotoxaemia are simulated by introducing combinations of two treatments, as well as concurrent administration of all three interventions. Because the model captures complex interactions among immune, thermal, pain, and cardiovascular components, the goal was to assess how the combined treatment protocols impact the predicted behaviour and compare with the outcomes from the individual therapy administrations.

Our results show that treatment combinations outperform individual intervention regimens. Exploring pairs of therapies shows that, for most subjects, all physiological signals trend to their nominal levels under simultaneous administration of LPS adsorption and vasopressors and with the combination of antipyretics and vasopressors. On the other hand, the qualitative variations in SBP behaviour discussed above also exist for combination interventions. Ultimately, the multimodal therapy administering LPS adsorption, antipyretics and vasopressors is the most effective way to relieve pain and bring about the recovery of temperature, HR and BP. Although these results are promising, more work is needed to understand the effects of combined treatments for sepsis patients.

## Limitations and future work

A limitation of our model is that it is calibrated over a short time course dictated by the time scale of the two experimental endotoxin studies, of duration 6 and 9 hr. The latter makes it difficult to assess its ability to track dynamics over days, which is a requirement for understanding the response to an infection.

In addition, there are several simplifying assumptions within the model. We assume that the endotoxin decays linearly and that it is uncoupled from the rest of the model. This model is appropriate for studying the response to a bolus LPS injection. However, the model needs additional components to predict response to an infection with a reproducing bacterium or virus. Another simplifying assumption is the lack of haemoperfusion during LPS adsorption. This treatment pumps blood out of the body, passing it through an extracorporeal circuit before it is returned to the circulation. This procedure affects cardiovascular dynamics, and a potential complication is hypotension (Garella & Lorch, 1980).

Our results show that sustained endotoxaemia associated with a pronounced NO increase eventually leads to vasodilatation, overpowering vasoconstriction induced by the pain response. The result is hypotension. In our 'simple' model, vasoconstriction is induced by the pain response, although we acknowledge that other pathways, including circulating hormones (Zhou *et al.* 2003; Majumder & Wu, 2014) or oxidative stress as a result of reactive oxygen species produced by innate immune cells to kill pathogens (Agita & Alsagaff, 2017), impact vascular resistance, and advise their inclusion in future studies. However, it should be noted that incorporating other vasoconstriction pathways probably does not change the hypotension prediction of the model in response to NO-mediated vasodilatation.

Feedback pathways can also be included to link the dynamics of temperature, infection and inflammation. As mentioned earlier, fever may serve an essential role in fighting an infection. The evidence suggests that aggressive treatment for body temperature higher than 38.5°C can negatively affect critically ill patients' recovery, decreasing their ability to successfully clear infections (Schulman *et al.* 2005). Furthermore, fever is beneficial in combating pathogens by limiting their reproduction, increasing the activity of many antibiotic classes, and increasing the innate immune response (Walter *et al.* 2016). We will account for these effects in future studies by incorporating interactions among fever, activated macrophages and the invading pathogen. Also, although we recognize the importance of IL-1$\beta$ in the thermal response, it is not included in the current model because data were not measured in the experimental studies. Even without this cytokine, the model performed well, capturing the temperature response; however, incorporating the fever-pathogen interplay in future work may require accounting for IL-1$\beta$ dynamics.

Other potential extensions of the model include a more thorough investigation of sepsis and septic shock, life-threatening conditions resulting from uncontrollable infection. Symptoms include low BP and rapid HR, and there can also be severe organ damage (Nguyen *et al.* 2006). Although our model can obtain accurate fits to the data for transient endotoxaemia and predict how an individual will respond to treatment for endotoxin sustained at a lower level, additional work is necessary to incorporate the effect of tissue damage on the inflammatory response in sepsis, as shown in the model by Chow *et al.* (2005).

There are several evolving phases of infection from early to later stages, including sepsis, severe sepsis and septic shock (Gotts & Matthay, 2016). These phases differ in several ways, including evidence of organ dysfunction and persistent hypotension. Our model currently does not distinguish between these phases. To extend the model to analyse its response to an infection, the model should be solved over longer timescales (days).

## Conclusions

The present study develops the first physiological mathematical model that explains the interactions in humans among inflammation, body temperature, pain, HR and SBP. The model successfully captures the time course of events observed during transient endotoxaemia in healthy individuals reported in two independent experimental studies. Both studies examine the inflammatory and physiological responses to a one-time administration of bacterial endotoxin. We simulated a sustained pathological input scenario, which suggests that untreated, sustained endotoxin can bring about abnormally elevated HR and low SBP. Simulation analysis of therapeutic interventions shows that, to remedy these detrimental effects, the most effective approach is to administer a multimodal treatment combining endotoxin removal with antipyretics and vasopressors to simultaneously target LPS, pain, fever and vascular resistance.

## Appendix

### Model summary

The model described above forms a system of delay differential equations given by

$$\frac{dx}{dt} = f(x, t, t-\kappa;\ \theta), \tag{A1}$$

where $x = \{x_{inf}, x_{reg}, x_{cv}\}$ is the vector of model states ($x \in R^{20}$) and $\theta = \{\theta_{inf}, \theta_{reg}, \theta_{cv}\}$ is the vector of parameters ($\theta \in R^{88}$). The subscripts *inf*, *reg* and *cv* represent the inflammatory, regulatory, and cardiovascular submodels, respectively. That is

$$\begin{aligned} x_{inf} &= \{E, M_R, M_A, \text{TNF}, \text{IL6}, \text{IL8}, \text{IL10}\} \\ x_{reg} &= \left\{T\text{emp}, \text{PT}, \text{NO}(\text{t}-\kappa), R_s, H\right\} \\ x_{cv} &= \{V_{la}, V_{lv}, V_{ao}, V_{vo}\}. \end{aligned} \tag{A2}$$

The system contains one discrete delay $\kappa$ needed to predict activation/inhibition of NO from TNF-$\alpha$ and IL-10. In addition to the delay parameter $\kappa$, the system is described using the parameters $\theta$ including

$$\begin{aligned} \theta_{inf} = \{&k_E, k_M, k_{M\text{TNF}}, k_{MR}, k_{MA}, M_\infty, \eta_{ME}, h_{ME}, \\ &\eta_{M\text{TNF}}, h_{M\text{TNF}}, \eta_{M10}, h_{M10}, k_{\text{TNF}M}, k_{\text{TNF}}, \\ &\eta_{\text{TNF6}}, h_{\text{TNF6}}, \eta_{\text{TNF10}}, h_{\text{TNF10}}, w_{\text{TNF}}, k_{6M}, \\ &k_6, k_{6\text{TNF}}, \eta_{6\text{TNF}}, h_{6\text{TNF}}, \eta_{66}, h_{66}, \eta_{610}, h_{610}, \\ &w_{\text{IL6}}, k_{8M}, k_8, k_{8\text{TNF}}, \eta_{8\text{TNF}}, h_{8\text{TNF}}, \eta_{810}, \\ &h_{810}, w_{\text{IL8}}, k_{10M}, k_{10}, k_{106}, \eta_{106}, h_{106}, w_{\text{IL10}}\} \\ \theta_{reg} = \{&\tau_1, k_T, k_{T\text{TNF}}, k_{T6}, k_{T10}, T_b, T_M, \eta_{T\text{TNF}}, \\ &\eta_{T6}, \eta_{T10}, h_{T\text{TNF}}, h_{T6}, h_{T10}, k_{\text{PTE}}, k_{\text{PT}}, PT_b, \\ &k_{NM}, k_N, \eta_{N\text{TNF}}, h_{N\text{TNF}}, \eta_{N10}, h_{N10}, \\ &k_{RPT}, k_{RN}, k_R, \eta_{RPT}, R_b \\ &\tau_2, k_H, H_b, H_M, BP_b, \eta_{HT}, h_{HT}, \eta_{HP}, h_{HP}\} \\ \theta_{cv} = \{&R_{la}, R_{lv}, E_{la}, E_{lv}, E_{sa}, E_{sv}, V_{stroke}, E_m, E_M\}. \end{aligned} \tag{A3}$$

Table 1 lists all model parameters along with units and a description of their function. The delay differential equations listed above are solved in MATLAB using dde23 with an integration tolerance of $10^{-8}$.

### Inflammatory response

The equations of the inflammatory response are given by

$$\begin{aligned} \frac{dE}{dt} &= -k_E E \\ \frac{dM_R}{dt} &= -H_M^U(E)\left(k_M + k_{MTNF}H_M^U(TNF)\right) \\ &\quad H_M^D(IL10)M_R + k_{MR}M_R\left(1 - \frac{M_R}{M_\infty}\right) \\ \frac{dM_A}{dt} &= H_M^U(E)\left(k_M + k_{MTNF}H_M^U(TNF)\right)H_M^D \\ &\quad (IL10)M_R - k_{MA}M_A \\ \frac{dTNF}{dt} &= k_{TNFM}H_{TNF}^D(IL6)H_{TNF}^D \\ &\quad (IL10)M_A - k_{TNF}(TNF - w_{TNF}) \\ \frac{dIL6}{dt} &= \left(k_{6M} + k_{6TNF}H_{IL6}^U(TNF)\right)H_{IL6}^D(IL6)H_{IL6}^D \\ &\quad (IL10)\ M_A - k_6(IL6 - w_{IL6}) \\ \frac{dIL8}{dt} &= \left(k_{8M} + k_{8TNF}H_{IL8}^U(TNF)\right)H_{IL8}^D \\ &\quad (IL10)\ M_A - k_8(IL8 - w_{IL8}) \\ \frac{dIL10}{dt} &= \left(k_{10M} + k_{106}H_{IL10}^U(IL6)\right)\ M_A - k_{10} \\ &\quad (IL10 - w_{IL10}), \end{aligned} \tag{A4}$$

where the up- and down-regulation of Y by X is modelled using the Hill functions, $H_Y^U(X) = \frac{X^h}{\eta_{YX}^h + X^h}$ and $H_Y^D(X) = \frac{\eta_{YX}^h}{\eta_{YX}^h + X^h}$, respectively. Full model details are given in the study by Brady *et al.* (Brady *et al.* 2018).

### Cardiovascular response

The change in volume in the large and small arteries and veins are

$$\begin{aligned} &\frac{dV_{la}}{dt} = Q - q_a,\ \frac{dV_{sa}}{dt} = q_a - q_s,\ \frac{dV_{sv}}{dt} = q_s - q_v, \\ &\frac{dV_{lv}}{dt} = q_v - Q. \end{aligned} \tag{A5}$$

The flow through each compartment is found using Ohm's law giving

$$q_{la} = \frac{p_{la} - p_{sa}}{R_a},\ q_s = \frac{p_{sa} - p_{sv}}{R_s},\ q_{lv} = \frac{p_{sv} - p_{lv}}{R_v}, \tag{A6}$$

where $R_a$ and $R_v$ are arterial and venous resistances, and $R_s$ is the peripheral resistance.

For each cardiovascular compartment, the pressure and volume are related by

$$p_i - p_{tis} = E_i\ (V_i - V_{un}), \tag{A7}$$

where $V_i$ is the total and $V_{un}$ is the unstressed volume, $E_i$ is the elastance of the compartment, $p_i$ is the pressure in the compartment and $p_{tis}$ is the tissue pressure.

### Therapeutic interventions

We perform a theoretical therapy study over a 12 hr time window.

*Sustained endotoxaemia* is simulated by assuming that the amount of endotoxin ($E$) remains constant for 12 hr

$$\frac{dE}{dt} = 0. \tag{A8}$$

*LPS Adsorption* is administered after 4 hr of sustained endotoxin presence. As this therapy helps to remove LPS from the bloodstream, we increase the rate of endotoxin clearance and model this as

$$\frac{dE}{dt} = \begin{cases} 0, & \text{if } t \le 4 \\ -2k_E E, & \text{if } t > 4. \end{cases} \tag{A9}$$

There is a constant, sustained level of endotoxin initially, which begins to decay once LPS adsorption is introduced at $t = 4$ hr. The decay rate is set to be twice as fast as the endotoxin would decay during transient endotoxaemia without intervention with LPS adsorption.

*Antipyretics* are also introduced into the model at $t = 4$ hr. We model the effect of antipyretics by modifying the equations for PT and temperature (Temp). We reduce the rate at which endotoxin lowers PT, as well as the rates at which TNF-$\alpha$ and IL-6 upregulate body temperature

$$\frac{d\mathrm{PT}}{dt} = \begin{cases} -k_{\mathrm{PT}E} E\ PT + k_{\mathrm{PT}}\left(PT_b - \mathrm{PT}\right), & \text{if } t \le 4 \text{ or } 7 < t \le 10 \\ -0.1\ k_{\mathrm{PT}E} E\ PT + k_{\mathrm{PT}}\left(PT_b - \mathrm{PT}\right), & \text{if } 4 < t \le 7 \text{ or } 10 < t \le 12 \end{cases} \tag{A10}$$

$$\frac{d\mathrm{Temp}}{dt} = \begin{cases} \frac{1}{\tau_1}(-\mathrm{Temp} + T_b + k_T\left(T_M - T_b\right)\left(k_{T\mathrm{TNF}} H_T^U\left(|\mathrm{TNF} - w_{\mathrm{TNF}}|\right)\right. \\ \left. + k_{T6} H_T^U\left(|\mathrm{IL6} - w_{\mathrm{IL6}}|\right)\left(-k_{T10}\left(1 - H_T^D\left(|\mathrm{IL10} - w_{\mathrm{IL10}}|\right)\right)\right), & \text{if } t \le 4 \text{ or } 7 < t \le 10 \\ \frac{1}{\tau_1}(-\mathrm{Temp} + T_b + k_T\left(T_M - T_b\right)\left(0.1 k_{T\mathrm{TNF}} H_T^U\left(|\mathrm{TNF} - w_{\mathrm{TNF}}|\right)\right. \\ \left. + 0.1 k_{T6} H_T^U\left(|\mathrm{IL6} - w_{\mathrm{IL6}}|\right)\left(-k_{T10}\left(1 - H_T^D\left(|\mathrm{IL10} - w_{\mathrm{IL10}}|\right)\right)\right), & \text{if } 4 < t \le 7 \text{ or } 10 < t \le 12. \end{cases}$$

*Vasopressors* are also introduced after 4 hr of sustained endotoxaemia. Their action leads to an increase in peripheral vascular resistance ($R_s$). We model this effect by letting the peripheral vascular resistance approach its baseline value ($R_b$) more quickly

$$\frac{dR_s}{dt} = \begin{cases} k_{RPT}\dfrac{\Gamma^2}{\Gamma^2 + \eta^2{}_{RPT}} - k_{RN}N - k_R\left(R_s - R_b\right), & \text{if } t \le 4 \\ k_{RPT}\dfrac{\Gamma^2}{\Gamma^2 + \eta^2{}_{RPT}} - k_{RN}N - (2)\cdot k_R\left(R_s - R_b\right), & \text{if } t > 4. \end{cases} \tag{A11}$$

*Multimodal Treatments*, also initiated 4 hr after sustained presence of endotoxin, consist of the following combinations of treatments: (i) LPS adsorption and antipyretics (eqns (A9–A10)); (ii) LPS adsorption and vasopressors (eqns (A9) and (A11)); (iii) Antipyretics and vasopressors (eqns (A10) and (A11)); and (d) LPS adsorption, antipyretics and vasopressors (eqns (A9)–(A11)).

## References


Agita A & Alsagaff MT (2017). Inflammation, immunity, and hypertension. *Acta Med Indones* **49**, 158–165.

An G (2006). Concepts for developing a collaborative in silico model of the acute inflammatory response using agent-based modeling. *J Crit Care* **21**, 105–110.

Arndt JO, Morgenstern J & Samodelov L (1977). The physiologically relevant information regarding systemic blood pressure encoded in the carotid sinus baroreceptor discharge pattern. *J Physiol* **268**, 775–791.

Benson S, Kattoor J, Wegner A, Hammes F, Reidick D, Grigoleit JS, Engler H, Oberbeck R, Schedlowski M & Elsenbruch S (2012). Acute experimental endotoxemia induces visceral hypersensitivity and altered pain evaluation in healthy humans. *Pain* **153**, 794–799.

Bogdan C (2001). Nitric oxide and the immune response. *Nat Immunol* **2**, 907–916.

Bogdan C (2015). Nitric oxide synthase in innate and adaptive immunity: an update. *Trends Immunol* **36**, 161–178.

Borovikova LV, Ivanova S, Zhang M, Yang H, Botchkina GI, Watkins LR, Wang H, Abumrad N, Eaton JW & Tracey KJ (2000). Vagus nerve stimulation attenuates the systemic inflammatory response to endotoxin. *Nature* **405**, 458–462.

Brady R (2017). In *Mathematical modeling of the acute inflammatory response and cardiovascular dynamics in young men*. Raleigh, NC 27695: Department of Mathematics, North Carolina State University.

Brady R & Enderling H (2019). Mathematical models of cancer: when to predict novel therapies, and when not to. *Bull Math Biol* **81**, 3722–3731.

Brady R, Frank-Ito DO, Tran HT, Janum S, Møller K, Brix S, Ottesen JT, Mehlsen J & Olufsen MS (2018). Personalized mathematical model of endotoxin-induced inflammatory responses in young men and associated changes in heart rate variability. *Math Model Nat Phenom* **13**, 42.

Brown B, Price I, Toapanta F, DeAlmeida D, Wiley C, Ross T, Oury T & Vodovotz Y (2011). An agent-based model of inflammation and fibrosis following particulate exposure in the lung. *Math Biosci* **231**, 186–196.

Bruehl S, Chung O, Ward P, Johnson B & McCubbin J (2002). The relationship between resting blood pressure and acute pain sensitivity in healthy normotensives and chronic back pain sufferers: the effects of opioid blockade. *Pain* **100**, 191–201.

Cao WW & Morrison S (2003). Disinhibition of rostral raphe pallidus neurons increases cardiac sympathetic nerve activity and heart rate. *Brain Res* **980**, 1–10.

Chavan SS, Pavlov VA & Tracey KJ (2017). Mechanisms and therapeutic relevance of neuro-immune communication. *Immunity* **46**, 927–942.

Chesrown SE, Monnier J, Visner G & Nick HS (1994). Regulation of inducible nitric oxide synthase mRNA levels by LPS, INF-$\gamma$, TGF-$\beta$, and IL-10 in murine macrophage cell lines and rat peritoneal macrophages. *Biochem Biophys Res Commun* **200**, 126–134.

Chow CC, Clermont G, Kumar R, Lagoa C, Tawadrous Z, Gallo D, Betten B, Bartels J, Constantine G, Fink MP, Billiar TR & Vodovotz Y (2005). The acute inflammatory response in diverse shock states. *Shock* **24**, 74–84.

Conti B, Tabarean I, Andrei C & Bartfai T (2004). Cytokines and fever. *Front Biosci* **9**, 1433–1449.

Copeland S, Warren HS, Lowry SF, Calvano SE & Remick D (2005). Acute inflammatory response to endotoxin in mice and humans. *Clin Diagn Lab Immunol* **12**, 60–67.

Coussens LM & Werb Z (2002). Inflammation and cancer. *Nature* **420**, 860–867.

Crandall CG, Zhang R & Levine B (2000). Effects of whole body heating on dynamic baroreflex regulation of heart rate in humans. *Am J Physiol Heart Circ Physiol* **279**, H2486–H2492.

Crandall CG & Wilson TE (2015). Human cardiovascular responses to passive heat stress. *Compr Physiol* **5**, 17–43.

Daun S, Rubin J, Vodovotz Y, Roy A, Parker R & Clermont G (2008). An ensemble of models of the acute inflammatory response to bacterial lipopolysaccharide in rats: results from parameter space reduction. *J Theor Biol* **253**, 843–853.

Dong X, Foteinou P, Calvano S, Lowry S & Androulakis I (2010). Agent-based modeling of endotoxin-induced acute inflammatory response in human blood leukocytes. *PLoS One* **5**, e9249.

Evans SS, Repasky EA & Fisher DT (2015). Fever and the thermal regulation of immunity: the immune system feels the heat. *Nat Rev Immunol* **15**, 335–349.

Fink MP (2014). Animal models of sepsis. *Virulence* **5**, 143–153.

Foteinou PT, Calvano SE, Lowry SF & Androulakis IP (2011). A physiological model for autonomic heart rate regulation in human endotoxemia. *Shock* **35**, 229–239.

Garella S & Lorch JA (1980). Hemoperfusion for acute intoxications: con. *Clin Toxicol* **17**, 515–527.

Gellish RL, Goslin BR, Olson RE, McDonald A, Russi GD & Moudgil VK (2007). Longitudinal modeling of the relationship between age and maximal heart rate. *Med Sci Sports Exerc* **39**, 822–829.

Gotts JE & Matthay MA (2016). Sepsis: pathophysiology and clinical management. *BMJ* **353**, i1585

Hall JE (2015). *Guyton and Hall Textbook of Medical Physiology*. WB Saunders Co, Philadelphia, PA.

Hamzic N, Tang Y, Eskilsson A, Kugelberg U, Ruud J, Jönsson JI, Blomqvist A & Nilsberth C (2013). Interleukin-6 primarily produced by non-hematopoietic cells mediates the lipopolysaccharide-induced febrile response. *Brain Behav Immun* **33**, 123–130.

Haskó G, Szabó C, Németh ZH, Kvetan V, Pastores SM & Vizi ES (1996). Adenosine receptor agonists differentially regulate IL-10, TNF-alpha, and nitric oxide production in RAW 264.7 macrophages and in endotoxemic mice. *J Immunol* **157**, 4634–4640.

Hotchkiss RS & Karl IE (2003). The pathophysiology and treatment of sepsis. *N Engl J Med* **348**, 138–150.

Howell MD & Davis AM (2017). Management of sepsis and septic shock. *JAMA* **317**, 847–848.

Hoyert DL & Xu J (2012). Deaths: preliminary data for 2011. *Natl Vital Stat Rep* **61**, 1–51.

Hudsmith L, Petersen SE, Francis JM, Robson MD & Neubauer S (2005). Normal human left and right ventricular and left atrial dimensions using steady state free precession magnetic resonance imaging. *J Cardiovasc Magn Reson* **7**, 775–782.

Huston JM & Tracey KJ (2011). The pulse of inflammation: heart rate variability, the cholinergic anti-inflammatory pathway and implications for therapy. *J Intern Med* **269**, 45–53.

Huston JM, Wang H, Ochani M, Ochani K, Rosas-Ballina M, Gallowitsch-Puerta M, Ashok M, Yang L, Tracey KJ & Yang H (2008). Splenectomy protects against sepsis lethality and reduces serum HMGB1 levels. *J Immunol* **181**, 3535–3539.

Janum S, Nielsen S, Werner M, Mehlsen J, Kehlet H & Møller K (2016). Pain perception in healthy volunteers: effect of repeated exposure to experimental systemic inflammation. *Innate Immun* **22**, 546–556.

Karjalainen J & Viitasalo M (1986). Fever and cardiac rhythm. *Arch Intern Med* **146**, 1169–1171.

Kirkebøen KA & Strand OA (1999). The role of nitric oxide in sepsis–an overview. *Acta Anaesthesiol Scand* **43**, 275–288.

Korner PI, Tonkin AM & Uther JB (1976). Reflex and mechanical circulatory effects of graded Valsalva maneuvers in normal man. *J Appl Physiol* **40**, 434–440.

La Rovere MT, Pinna GD & Raczak G (2008). Baroreflex sensitivity: measurement and clinical Implications. *Ann Noninvasive Electrocardiol* **13**, 191–207.

Lai N, Mills K & Chiu I (2017). Sensory neuron regulation of gastrointestinal inflammation and bacterial host defence. *J Intern Med* **282**, 5–23.

Lazarus M, Yoshida K, Coppari R, Bass CE, Mochizuki T, Lowell BB & Saper CB (2007). EP3 prostaglandin receptors in the median preoptic nucleus are critical for fever responses. *Nat Neurosci* **10**, 1131–1133.

Lepper PM, Held TK, Schneider EM, Bölke E, Gerlach H & Trautmann M (2002). Clinical implications of antibiotic-induced endotoxin release in septic shock. *Intensive Care Med* **28**, 824–833.

Lundberg J, Gladwin M & Weitzberg E (2015). Strategies to increase nitric oxide signalling in cardiovascular disease. *Nat Rev Drug Discov* **14**, 623–641.

Maixner W, Gracely R, Zuniga J, Humphrey C & Bloodworth G (1990). Cardiovascular and sensory responses to forearm ischemia and dynamic hand exercise. *Am J Physiol Regul Integr Comp Physiol* **259**, R1156–R1163.

Majumder K & Wu J (2014). Molecular targets of anti-hypertensive peptides: understanding the mechanisms of action based on the pathophysiology of hypertension. *Int J Mol Sci* **16**, 256–283.

Mathews J & Fink K (2004). *Numerical Methods Using MATLAB*, Pearson, Upper Saddle River, NJ.

McDaniel M, Keller J, White S & Baird A (2019). A whole-body mathematical model of sepsis progression and treatment designed in the BioGears physiology engine. *Front Physiol* **10**, 1321.

McNeill E, Crabtree MJ, Sahgal N, Patel J, Chuaiphichai S, Iqbal AJ, Hale AB, Greaves DR & Channon KM (2015). Regulation of iNOS function and cellular redox state by macrophage Gch1 reveals specific requirements for tetrahydrobiopterin in NRF2 activation. *Free Radic Biol Med* **79**, 206–216.

Nakamura K, Matsumura K, Hübschle T, Nakamura Y, Hioki H, Fujiyama F, Boldogköi Z, König M, Thiel H-J, Gerstberger R, Kobayashi S & Kaneko T (2004). Identification of sympathetic premotor neurons in medullary raphe regions mediating fever and other thermo-regulatory functions. *J Neurosci* **24**, 5370–5380.

Nguyen HB, Rivers EP, Abrahamian FM, Moran GJ, Abraham E, Trzeciak S, Huang DT, Osborn T, Stevens D & Talan DA (2006). Severe sepsis and septic shock: review of the literature and emergency department management guidelines. *Ann Emerg Med* **48**, 28–54.

Niven DJ, Stelfox HT & Laupland KB (2013). Antipyretic therapy in febrile critically ill adults: a systematic review and meta-analysis. *J Crit Care* **28**, 303–310.

Olufsen MS & Ottesen JT (2013). A practical approach to parameter estimation applied to model predicting heart rate regulation. *J Math Biol* **67**, 39–68.

Oyetunji TA, Chang DC, Crompton JG, Greene WR, Efron DT, Haut ER, Cornwell EEr & Haider AH (2011). Redefining hypotension in the elderly: normotension is not reassuring. *Arch Surg* **146**, 865–869.

Park H & Pyo S (2013). LPS-induced autophagy is mediated by nitric oxide in macrophages (P1285). *J Immunol* **190**, 56.25.

Pajkrt D, van der Poll T, Levi M, Cutler DL, Affrime MB, van den Ende A, ten Cate JW & van Deventer SJ (1997). Interleukin-10 inhibits activation of coagulation and fibrinolysis during human endotoxemia. *Blood* **89**, 2701–2705.

Pilling D, Galvis-Carvajal E, Karhadkar T, Cox N & Gomer R (2017). Monocyte differentiation and macrophage priming are regulated differentially by pentraxins and their ligands. *BMC Immunol* **18**, 30.

Pinho-Ribeiro F, Verri JW & Chiu I (2017). Nociceptor sensory neuron–immune interactions in pain and inflammation. *Trends Immunol* **38**, 5–19.

Plaisance KI & Mackowiak PA (2000). Antipyretic therapy: physiologic rationale, diagnostic implications, and clinical consequences. *Arch Intern Med* **160**, 449–456.

Prince JM, Levy RM, Bartels J, Baratt A, Kane JMr, Lagoa C, Rubin J, Day J, Wei J, Fink MP, Goyert SM, Clermont G, Billiar TR & Vodovotz Y (2006). In silico and in vivo approach to elucidate the inflammatory complexity of CD14-deficient mice. *Mol Med* **12**, 88–96.

Randall EB, Billeschou A, Brinth LS, Mehlsen J & Olufsen MS (2019). A model-based analysis of autonomic nervous function in response to the Valsalva maneuver. *J Appl Physiol* **127**, 1386–1402.

Riedel W, Städter WR & Gray DA (1986). Activation of thyrotropinreleasing hormone (TRH) neurons by cold or after thyroidectomy inhibits antidiuretic hormone (ADH) secretion in febrile rabbits. *J Auton Nerv Syst* **13**, 543–552.

Roti Roti JL (2008). Cellular responses to hyperthermia (40-46 degrees C): cell killing and molecular events. *Int J Hyperthermia* **24**, 3–15.

Rudiger A & Singer M (2013). The heart in sepsis: from basic mechanisms to clinical management. *Curr Vasc Pharmacol* **11**, 187–195.

Russell JA (2006). Management of sepsis. *N Engl J Med* **355**, 1699–1713.

Saccò M, Meschi M, Regolisti G, Detrenis S, Bianchi L, Bertorelli M, Pioli S, Magnano A, Spagnoli F, Giuri P, Fiaccadori E & Caiazza A (2013). The relationship between blood pressure and pain. *J Clin Hypertens* **15**, 600–605.

Salim T, Sershen C & May E (2016). Investigating the role of TNF-$\alpha$ and IFN-$\gamma$ activation on the dynamics of iNOS gene expression in LPS stimulated macrophages. *PLoS One* **11**, e0153289.

Sayk F, Vietheer A, Schaaf B, Wellhoener P, Weitz G, Lehnert H & Dodt C (2008). Endotoxemia causes central down-regulation of sympathetic vasomotor tone in healthy humans. *Am J Physiol Regul Integr Comp Physiol* **295**, R891–R898.

Scheff JD, Mavroudis PD, Calvano SE, Lowry SF & Androulakis IP (2011). Modeling autonomic regulation of cardiac function and heart rate variability in human endotoxemia. *Physiol Genomics* **43**, 951–964.

Schulman CI, Namias N, Doherty J, Manning RJ, Li P, Elhaddad A, Lasko D, Amortegui J, Dy CJ, Dlugasch L, Baracco G & Cohn SM (2005). The effect of antipyretic therapy upon outcomes in critically ill patients: a randomized, prospective study. *Surg Infect* **6**, 369–375.

Seok J, Warren HS, Cuenca AG, Mindrinos MN, Baker HV, Xu W, Richards DR, McDonald-Smith GP, Gao H, Hennessy L, Finnerty CC, López CM, Honari S, Moore EE, Minei JP, Cuschieri J, Bankey PE, Johnson JL, Sperry J, Nathens AB, Billiar TR, West MA, Jeschke MG, Klein MB, Gamelli RL, Gibran NS, Brownstein BH, Miller-Graziano C, Calvano SE, Mason PH, Cobb JP, Rahme LG, Lowry SF, Maier RV, Moldawer LL, Herndon DN, Davis RW, Xiao W & Tompkins RG (2013). Genomic responses in mouse models poorly mimic human inflammatory diseases. *Proc Natl Acad Sci U S A* **110**, 3507–3512.

Shinar Z, Akselrod S, Dagan Y & Baharav A (2006). Autonomic changes during wake sleep transition: a heart rate variability based approach. *Auton Neurosci* **130**, 17–27.

Toussaint K, Yang XC, Zielinski MA, Reigle KL, Sacavage SD, Nagar S & Raffa RB (2010). What do we (not) know about how paracetamol (acetaminophen) works? *J Clin Pharm Ther* **35**, 617–638.

Tracey K (2002). The inflammatory reflex. *Nature* **420**, 853–859.

Tracey K (2011). Ancient neurons regulate immunity. *Science* **332**, 673–674.

Tripathi P, Tripathi P, Kashyap L & Singh V (2007). The role of nitric oxide in inflammatory reactions. *FEMS Immunol Med Microbiol* **51**, 443–452.

Vayssettes-Courchay C, Bouysset F & Verbeuren TJ (2005). Sympathetic activation and tachycardia in lipopolysaccharide treated rats are temporally correlated and unrelated to the baroreflex. *Auton Neurosci* **120**, 35–45.

Victorino GP, Battistella FD & Wisner DH (2003). Does tachycardia correlate with hypotension after trauma? *J Am Coll Surg* **196**, 679–684.

Walter EJ, Hanna-Jumma S, Carraretto M & Forni L (2016). The pathophysiological basis and consequences of fever. *Crit Care* **20**, 200.

Warner H & Cox A (1962). A mathematical model of heart rate control by sympathetic and vagus efferent information. *J Appl Physiol* **17**, 349–355.

Wegner A, Elsenbruch S, Maluck J, Grigoleit JS, Engler H, Jäger M, Spreitzer I, Schedlowski M & Benson S (2014). Inflammation-induced hyperalgesia: effects of timing, dosage, and negative affect on somatic pain sensitivity in human experimental endotoxemia. *Brain Behav Immun* **41**, 46–54.

Wei X, Song H, Yin L, Rizzo M, Sidhu R, Covey D, Ory D & Semenkovich C (2016). Fatty acid synthesis configures the plasma membrane for inflammation in diabetes. *Nature* **539**, 294–298.

Williams N, Brady R, Gilmore S, Gremaud P, Tran H, Ottesen J, Mehlsen J & Olufsen M (2019). Cardiovascular dynamics during head-up tilt assessed via pulsatile and non-pulsatile models. *J Math Biol* **79**, 987–1014.

Yamanaka Y, Uchida K, Akashi M, Watanabe Y, Yaguchi A, Shimamoto S, Shimoda S, Yamada H, Yamashita M & Kimura H (2019). Mathematical modeling of septic shock based on clinical data. *Theor Biol Med Model 1* **16**, 15.

Yamazaki F, Sagawa S, Torii R, Endo Y & Shiraki K (1997). Effects of acute hyperthermia on the carotid baroreflex control of heart rate in humans. *Int J Biometeorol* **40**, 200–205.

Yaroustovsky M, Abramyan M, Komardina E, Nazarova H, Popov D, Plyushch M, Soldatkina A & Rogalskaya E (2018). Selective LPS adsorption using polymyxin B-immobilized fiber cartridges in sepsis patients following cardiac surgery. *Shock* **49**, 658–666.

Yudkin J, Kumari M, Humphries S & Mohamed-Ali V (2000). Inflammation, obesity, stress and coronary heart disease: is interleukin-6 the link? *Atherosclerosis* **148**, 209–214.

Zhang YH, Lu J, Elmquist JK & Saper CB (2000). Lipopolysaccharide activates specific populations of hypothalamic and brainstem neurons that project to the spinal cord. *J Neurosci* **20**, 6578–6586.

Zhou Y, Chen Y, Dirksen WP, Morris M & Periasamy M (2003). AT1b receptor predominantly mediates contractions in major mouse blood vessels. *Circ Res* **93**, 1089–1094.

## Additional information

### Data availability statement

This manuscript uses cytokine and physiological data from previously published studies (Copeland *et al.* 2005; Janum *et al.* 2016). The model is calibrated using individual Janum data from 20 healthy young men and is subsequently validated using averaged data reported in the Copeland study and average data from the Janum study. Time series data along with computer simulations for all subjects are included in Supplement 1.

Computer code for this project is available in the GitHub repository: https://github.com/msolufse/Inflammation-and-Cardiovascular-Dynamics.

### Competing interests

The authors declare that they have no competing interests.

### Author contributions

AD, RB-N, KL, CP and MSO were responsible for the conception or design of the work. AD, RB-N, JM and MSO were responsible for acquisition, analysis or interpretation of data for the work. AD, RB-N, KL, CP, JM and MSO were responsible for drafting the work or revising it critically for important intellectual content. AD, RB-N, KL, CP, JM and MSO were responsible for approval of the final version of the manuscript. AD, RB-N, KL, CP, JM and MSO agree to be accountable for all aspects of the work. All persons designated as authors qualify for authorship and all those who qualify for authorship are listed.

## Funding

Dobreva and Olufsen were supported in part by NSF-RTG-1 246 991. Puelz was supported in part by the NSF/DMS-RTG-1 646 339. Brady-Nicholls was supported by The Jayne Koskinas Ted Giovanis Foundation for Health and Policy. Olufsen, Puelz, Larripa and Brady-Nicholls were also supported by the Mathematics Research Communities via an award to the AMS (NSF-DMS-1 321 794).

## Acknowledgements

We thank S. Janum, K. Møller and S. Brix for their contributions to the data collection process.

## Keywords

cardiovascular dynamics, immune response, mathematical modelling, parameter estimation, thermal regulation

## Supporting information

Additional supporting information may be found online in the Supporting Information section at the end of the article.

**Statistical Summary Document**
**Doc. S1**. A supplement showing results of simulations for all subjects included in the study. Results show results of the coupled cytokine-cardiovascular model fitted to data for each subject, and the individual response to each treatment studied.